Multi-Beam Patch Antenna Design

Mustafa Konca

Submitted to the
Institute of Graduate Studies and Research
in partial fulfillment of the requirements for the Degree of

Master of Science
in
Electrical and Electronic Engineering

Eastern Mediterranean University
May 2010
Gazimağusa, North Cyprus

Approval of the Institute of Graduate Studies and Research

Prof. Dr. Elvan Yılmaz
Director (a)

I certify that this thesis satisfies the requirements as a thesis for the degree of Master of Science in of Electrical and Electronic Engineering.

Assoc. Prof. Dr. Aykut Hocanın
Chair, Department of Electrical and Electronic Engineering

We certify that we have read this thesis and that in our opinion it is fully adequate in scope and quality as a thesis for the degree of Master of Science in Electrical and Electronic Engineering.

Prof. Dr. Şener Uysal
Supervisor

Examining Committee

1. Prof. Dr. Haluk Tosun
2. Prof. Dr. Şener Uysal
3. Assoc. Prof. Dr. Hasan Demirel

ABSTRACT

This thesis describes the design procedure of a circular microstrip antenna array to be used for wireless communications. The proposed antenna utilizes a novel feed network that enables the user to change the propagation direction by choosing one or more of the four input ports. Equilateral triangular patches are used as array elements to utilize the space efficiently around the circular feed network. Both the feed network and the radiating elements are placed on a 1.57 mm thick FR-4 substrate, which is suspended 5 mm above the ground plane. The antenna array is designed to operate at a center frequency of 2.45 GHz.

Results show that single beams at eight different directions can be obtained by exciting certain combinations of input ports. Other combinations allow the array to radiate simultaneously in two directions. The dual-beam operation is possible in two different configurations. The steering angle is around 10^{o} off the z-axis and the beamwidth is around 20^{o} for all of the main beams. Gain values of up to 8.3 dB were obtained.

Keywords: Circular antenna array, Triangular patch, Multi directional, Multi beam, Circular power divider.

ÖZ

Bu tez, dairesel şekilde dizilmiş eşkenar üçgen elemanlardan oluşan bir basılı devre anten dizisi tasarımı ve bilgisayar modellemesi sonuçlarını içerir. Söz konusu anten uzak noktalardaki birimlerin esnek bir şekilde birbirleri ile iletişim kurmasına yarayacaktır. Anten dizisinde kullanılan basılı devre besleme ağı özgün bir tasarım olup, her elemanı değişik bir faz ile besleyerek antenin yayın yönünün değişmesini sağlar. Bu dairesel besleme şeridi üzerinde sağlanan dört değişik noktadan her birinin veya birkaçının kullanılması sonucunda anten yayın yönü seçilebilmektedir. Hem besleme ağı hem de anten dizisi 1.57 mm kalınlığındaki bir FR-4 plaka üzerine basılacaktır. Bu devre plakası toprak düzleminin 5 mm üzerine monte edilecektir. Bu anten dizisi 2.45 GHz merkez frekansında çalışmak üzere tasarlanmıştır.

Sonuçlar, antenin değişik besleme noktaları kullanılarak, sekiz farklı yönde yayın yapabildiğini göstermiştir. Antenin aynı anda iki yöne yayın yapabilmesini sağlayan kombinasyonlar da mümkündür. Antenin yayın yönü yaklaşık olarak dikeyden 10 derece aşağıya kaydırılabilmektedir ve yayın alanı açısı yaklaşık olarak 20 derecedir. 8.3 dB'ye ulaşan kazanç değerleri elde edilmiştir.

Anahtar Kelimeler: Dairesel anten dizisi, Üçgen panel anten, Çok-yönlü yayın, Dairesel besleme ağı.

ACKNOWLEDGMENT

I would like to thank my supervisor, Prof. Dr. Şener Uysal, for his unconditional and enthusiastic support that he has given me throughout my thesis. He has broadened my horizon with his unique and innovative ideas, helping me to find solutions to challenging problems. This thesis wouldn't have been possible without Prof. Dr. Şener Uysal's guidance and invaluable supervision.

I would also like to thank my family for their endless support and faith in me. They have always strived to provide all the means that were necessary for me to get the best education. I am especially grateful to my father for his candid comments and fruitful discussions.

TABLE OF CONTENTS

ABSTRACT iii

ÖZ iv

ACKNOWLEDGMENT v

TABLE OF CONTENTS vi

LIST OF TABLES ix

LIST OF FIGURES x

1 INTRODUCTION 1

1.1 Antenna Basics 2

1.1.1 Some Fundamental Parameters and Equations 2

1.2 Thesis Objectives 7

1.2.1 Durability 7

1.2.2 High Gain 8

1.2.3 Coverage Area (Multiple Beams) 9

1.2.4 Selection of Transmission Band and Bandwidth 10

1.2.5 Efficiency 10

1.2.6 Affordability 10

1.3 Overview of Patch Antennas 11

1.3.1 History of Patch Antennas 11

1.3.2 Patch Antennas Today 11

1.3.3 Advantages and Disadvantages of Microstrip Antennas 13

2 THEORETICAL DESIGN 15

2.1 Transmission Line Model 15

2.1.1 Fringing Effects 16

2.2 Rectangular Patch 16

2.2.1 Design Parameters 17
2.2.2 Design Procedure and Calculations 17
2.3 Equilateral Triangular Patch Design 20
2.3.1 Design Procedure and Calculations 20
2.4 Array Theory and its Effects 21
2.4.1 Linear Phased Array 23
2.4.2 Butler Matrix 24
2.4.3 Rotman Bootlace Lens 25
3 SIMULATION AND DESIGN 26
3.1 Overview of the Utilized Software Packages 26
3.1.1 ADS 26
3.1.2 FEKO 27
3.2 Simple Rectangular Pin Fed Patch 27
3.3 Triangular Antenna Design 31
3.4 Circular Feed Network Design 34
3.4.1 Circular Divider Design using ADS 35
3.4.2 Circular Feed Network Design using FEKO 39
3.4.3 Comparison with other Feed Structures 42
3.5 Circular Array Design 43
3.5.1 Earlier Work 43
3.5.2 Array Structure and Simulation Parameters 43
3.5.3 Unmodified Circular Array Simulation Results 45
3.5.4 Improved Circular Array: Simulation Results 55
4 CONCLUSION and RECOMMENDATIONS 67
4.1 Conclusion 67

4.2 Recommendations and Future Work 67

REFERENCES 68

APPENDIX 73

FR-4 Substrate Properties 74

LIST OF TABLES

Table 1: Advantages and disadvantages of patch antennas. 13

Table 2: Comparison of properties of some antenna types. 14

Table 3: Change of radiation direction obtained through excitation of different port combinations 66

Table 4: Electrical properties of Fr-4 substrate 74

LIST OF FIGURES

Figure 1: Illustration of increasing gain as the coverage area (beamwidth) is reduced [6]. 3

Figure 2: Radiation pattern. 4

Figure 3: Half power beamwidth [6]..... 5

Figure 4: Bandwidth definition with respect to input reflection coefficient (S11). 6

Figure 5: An Internal Cell Phone Antenna. 12

Figure 6: A MSA in its commercial cover and a uniformly fed 4-element array. 13

Figure 7: The electric and magnetic fields in a microstrip structure. 15

Figure 8: A typical rectangular patch geometry. 17

Figure 9: Radiation pattern of a standard λ/2 long dipole antenna. 21

Figure 10: The effects of phase and array configuration on the radiation pattern of a standard /2 long dipole antenna [6]. 22

Figure 11: Linear antenna array showing the phase shifters and the shift in the direction of radiation through addition and cancellation of beams [6]. 23

Figure 12: A Butler Matrix with 4 input ports feeding 4 rectangular elements of a linear array [14]. 25

Figure 13: Rotman Bootlace Lens geometry from the original patent by W. Rotman [9]. 26

Figure 14: A physical Rotman Lens geometry [15]..... 26

Figure 15: Rectangular microstrip patch. 28

Figure 16: Input impedance of the pin fed rectangular patch. 29

Figure 17: Input reflection coefficient and the bandwidth of the pin fed rectangular patch. 30

Figure 18: 3-D radiation pattern of the rectangular pin-fed patch. 30

Figure 19: A cut-plane of the radiation pattern of the rectangular MSA. 31

Figure 20: Equilateral triangular MSA geometry. 32

Figure 21: Triangular antenna S11 performance results (FEKO). 33

Figure 22: 3-D radiation pattern of the equilateral triangular MSA. 33

Figure 23: Radiation pattern of the triangular MSA (plotted for $\Phi = 0^o$ and $\Phi = 90^o$) 34

Figure 24: Tuning wizard in ADS. 35

Figure 25: Circular feed network schematic generated using multilayer microstrip models of bends, tee junctions and straight lines in ADS. 1

Figure 26: Circular feed network layout generated using the schematic model in ADS and its dimensions as shown. 36

Figure 27: Circular feed network input reflection coefficient (S11) results from ADS. 37

Figure 28: Circular feed network output power level variations as computed in ADS, which shows what portion of the input power is transmitted to output terminals. 37

Figure 29: Circular feed network phase angles measured at the output ports using ADS. 39

Figure 30: Circular divider geometry in FEKO. 40

Figure 31: S11 results of the feed network simulated in FEKO. 40

Figure 32: Transmission coefficient results of the feed network simulated in FEKO. 41

Figure 33: Transmission coefficient results of the feed network simulated in FEKO. 42

Figure 34: Phase of the output ports of the feed network simulated in FEKO. 42

Figure 35: The circular array geometry composed of six equilateral triangular patches and the novel feed network. 44

Figure 36: Distribution of ports on the circular feed network. 45

Figure 37: Input reflection coefficient at port A, when it's the only excited port. 46

Figure 38: 3-D radiation pattern in linear scale, when only port A is excited. 47

Figure 39: Radiation pattern in decibel scale in $\Phi=0^{o}$ plane, when only port A is excited. 47

Figure 40: Input reflection coefficient at port A and port B. 48

Figure 41: Transmission coefficient (S21) between port A and B. 49

Figure 42: 3-D radiation pattern in linear scale, when port A and B are excited. 49

Figure 43: Radiation pattern in decibel scale in $\Phi=45^{o}$ plane, when ports A and B are excited. 50

Figure 44: 3-D radiation pattern in linear scale, when port A, B and C are excited.. 50

Figure 45: Radiation pattern in decibel scale in $\Phi=90^{o}$ plane, when ports A, B and C are excited. 51

Figure 46: Input reflection coefficient at ports A and C, when ports A, B and C are excited. 51

Figure 47: Input reflection coefficient at port B, when ports A, B and C are excited. 52

Figure 48: Transmission coefficients between ports A, B and C. 52

Figure 49: Input reflection coefficient at port A and port C, when ports A and C are excited. 53

Figure 50: 3-D radiation pattern in linear scale, when ports A and C are excited. 54

Figure 51: Radiation pattern in decibel scale in $\Phi=90^{o}$ plane, when ports A and C are excited. 54

Figure 52: Transmission coefficient between ports A and C. 55

Figure 53: Input reflection coefficient at port A, when it's the only excited port (after improvements). 56

Figure 54: Radiation pattern in decibel scale for phi = 0^{o}, when port A is excited (after improvements). 57

Figure 55: 3-D radiation pattern in linear scale, when port A is excited (after improvements). 57

Figure 56: Input reflection coefficient at port A, when it's the only excited port (after improvements). 58

Figure 57: Transmission coefficient (S21) between ports A and B (after improvements). 59

Figure 58: Radiation pattern in decibel scale for phi = 45^{o}, when ports A and B are excited (after improvements). 59

Figure 59: 3-D radiation pattern in linear scale, when ports A and B are excited (after improvements). 60

Figure 60: Input reflection coefficient at port A and C, when ports A, B and C are excited (after improvements). 60

Figure 61: Input reflection coefficient at port B, when ports A, B and C are excited (after improvements). 61

Figure 62: Isolation between the ports when ports A, B and C are excited (after improvements)..... 61

Figure 63: Radiation pattern in decibel scale for phi = 90^{o}, when ports A, B and C are excited (after improvements). 62

Figure 64: 3-D radiation pattern in linear scale, when ports A, B and C are excited (after improvements). 62

Figure 65: Input reflection coefficient at port A and port C, when ports A and C are excited (after improvements). 63

Figure 66: Transmission coefficient (S21) between ports A and C (after improvements)..... 63

Figure 67: Radiation pattern in decibel scale for phi = 0^{o}, when ports A and C are excited. 64

Figure 68: 3-D radiation pattern in linear scale, when ports A, B and C are excited (after improvements). 64

Figure 69: The final feed network dimensions. 65

Chapter 1

INTRODUCTION

The patch antenna, also called a micro-strip antenna (MSA), was first introduced in 50's [1] and started to receive considerable attention after 70's [2]. They were initially used for military applications such as planes and missiles but today they are widely used in civilian applications including cell phones, local area networks, multimedia devices and even microchips [3]-[5].

There is an ever growing demand for better and faster communication. While long distance Wi-Fi connections were rare in the past, they have become more common in the last decade. These types of connections are frequently used to create networks between buildings of an establishment or to connect standalone units at remote locations.

Arrays of MSA can easily be formed since they can be printed on a variety of substrates and conveniently connected through microstrip lines. MSA arrays can be utilized to improve the gain or bandwidth of a system but their benefits are revolutionary when they are utilized as smart arrays which have variable radiation patterns.

1.1 Antenna Basics

In this section, a concise coverage of antenna theory is given along with definitions of some key terms and several important equations that will help the reader to understand the terminology used in this document.

A simple definition of an antenna can be made as follows: a passive component which is physically an assembly of conductors and dielectrics, placed and shaped in a considerate manner. Although any piece of metal can be considered as an antenna, specific designs are required to radiate or receive signals at specific frequency ranges as effectively as possible. In another sense, an antenna is a coupling device between space (atmosphere) and a physical medium. The antenna can also be viewed as a matching network that takes the power from a transmission line (50 Ω, for example), and matches it to the free space "impedance" of 377 Ω.

1.1.1 Some Fundamental Parameters and Equations

The isotropic antenna: A theoretical antenna model that radiates equally in all directions and has a gain of 1 (0 dB). The isotropic antenna is a benchmark; the performance of other antennas is expressed in comparison to this antenna.

Directivity: The ratio of the radiation intensity in a given direction from the antenna to the radiation intensity averaged over all directions. If a direction is not specified with the directivity value, it is generally assumed that the direction of maximum intensity is implied [3]. For example, if the directivity of an antenna is 2 (3dB) in a certain direction, this means that it radiates twice as much power in that direction than an isotropic antenna would. A formula that defines directivity is given in Equation 1 and Figure 1 shows the relationship of directivity with the coverage area.

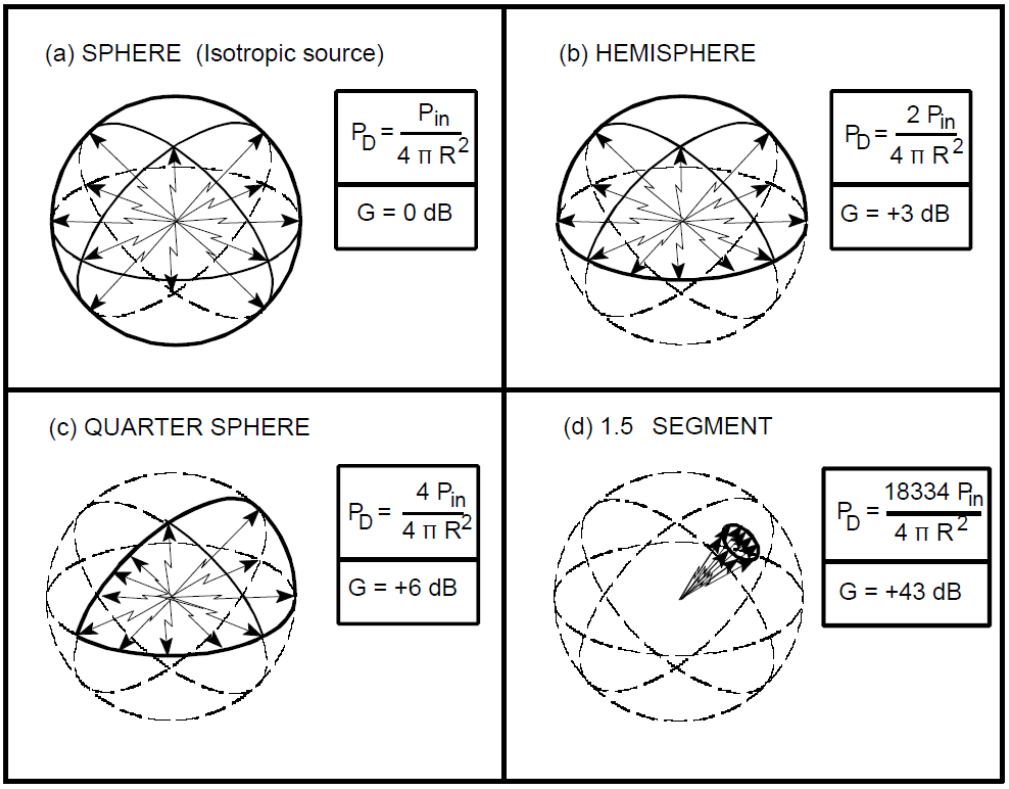

Figure 1: Illustration of increasing gain as the coverage area (beamwidth) is reduced [6].

Gain: This term gives the intensity of power transmitted in a certain direction after the losses are taken into account. The gain is closely related to the directivity of an antenna. In an ideal antenna, without losses, gain will equal directivity as the antenna efficiency factor equals 1 (100% efficiency). The symbol "η" is commonly used to represent efficiency of an antenna. Equation 2 gives the formula that can be used to derive gain by using directivity.

Radiation Pattern: A representation of the radiation properties of an antenna as a function of coordinates. This pattern can be modeled as a mathematical expression but usually it is graphically represented on a polar graph in decibels. The gain is the most commonly used parameter in expressing an antennas radiation pattern.

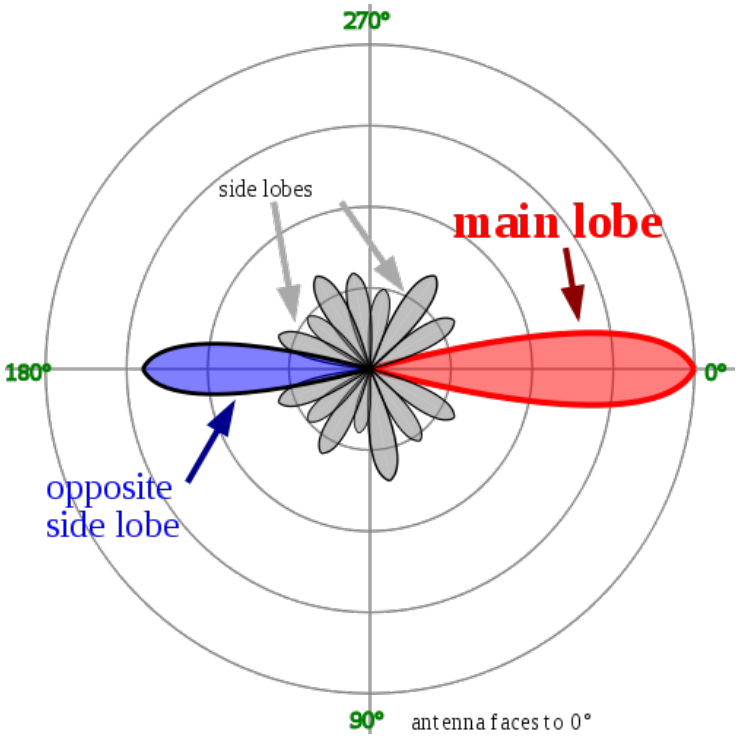

Figure 2: Radiation pattern.

Lobes: In a typical antenna's radiation pattern there are areas where radiation approaches zero and areas where there is a considerable amount of radiation. The areas of radiation are called the lobes (or sometimes beams) of an antenna. The radiation in the intended direction is represented by the main lobe as shown in Figure 2 and naturally, it's the strongest. But all practical antennas have losses and radiate energy in directions other than the intended direction. This radiation is represented by side lobes. Side lobes are generally unwanted and they should be kept at a minimum value. Side lobe power is given in decibels with respect to the maximum radiation.

Front to Back Ratio: The ratio of the energy radiated in the intended direction to the energy radiated in directly the opposite direction. This value is also expressed in decibels. It can also be defined as the ratio of the main lobe to the back lobe.

Beamwidth: The beamwidth of an antenna is the angle where the main lobe of the antenna covers. It is usually defined at the half power level. Also called the 3 dB beamwidth; pattern's angular width at the level where the gain is 3 dB down from the maximum. [7]

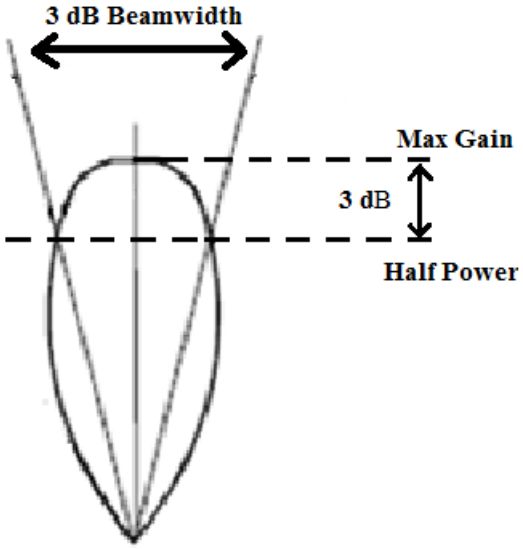

Figure 3: Half power beamwidth [6].

Bandwidth: The range of frequencies which the performance of an antenna exceeds a pre-set standard. Bandwidth can be expressed in Hertz or as a percentage of the center frequency. Generally, the bandwidth is defined as the frequency range where the antenna's input reflection coefficient (S_{11}) is lower than -10 dB.

Where f_1 and f_2 are the lower and upper band edge frequencies that meet the bandwidth criteria and f_c is the center frequency.

For example, the input reflection coefficient graph shown in Figure 4 indicates a bandwidth of 1 GHz, since the S11 is lower than -10 dB in the range of 2.5 to 3.5 GHz.

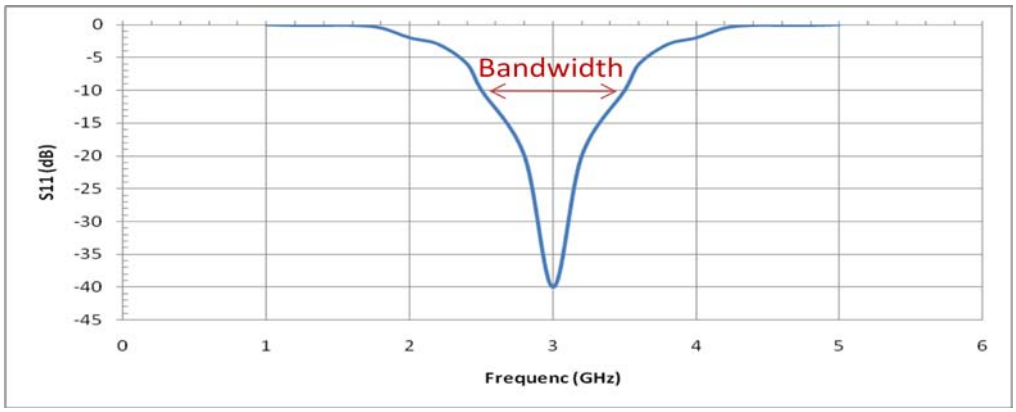

Figure 4: Bandwidth definition with respect to input reflection coefficient (S11).

Efficiency: A measure that shows what percent of the power is translated into useful radiation energy. Every antenna has certain input impedance. It is composed of Ohmic resistance which causes energy to turn to heat, radiation resistance which determines the ratio of power that is radiated and the reactance which can be either capacitive or inductive. The reactance needs to be kept at minimum. Ideally, an antenna should have a real input impedance of 50 Ω which would give the best performance since it will become a matched load. In this case any power dissipated for any other purpose than radiation is considered lost power [7] and this is given by Equation 4.

Antenna Array: An antenna array is formed by combination of more than one antenna in order to achieve a specific radiation performance. Array elements can be fed by a signal with the same power and phase which usually results in higher gain and narrower beamwidth. However, these parameters (mostly phase) can varied between the elements to achieve a specific pattern. These are called phased arrays and they can be of two types: active and passive. Active phased arrays make use of phase shifters and other solid state devices to vary the phase and power received by each element in the array. Passive arrays do not use any controlled devices and phase shifts are usually created using feeds of different length. Active arrays are more flexible and offer better performance due to their variable nature but they are costly and complicated structures which are more suspect to fault. On the other hand, a passive array is considerably cheaper and easier to build.

1.2 Thesis Objectives

The goal of this thesis is to present a novel antenna design that can be used for long range wireless communication between multiple units at remote locations. Some of the prerequisites needed to enable this type of a communication system are durability, weather proof design, low maintenance requirement, high gain, wide coverage area, wide bandwidth and high efficiency. Also, just like in any other practical design, cost and ease of manufacturability are very important factors especially when numerous units are required. It will be explained in the following sections why a patch antenna array, as presented in this thesis, would be the best choice in order to satisfy the mentioned requirements.

1.2.1 Durability

Durability is one of the most important requirements since the antennas are intended for use at remote locations on systems such as autonomous security modules or fire

surveillance networks. This requirement can most successfully be met by a patch antenna, while some of the other requirements such as high gain can also be met by other types of antennas. Also, the maintenance would be infrequent in such a scenario; therefore, a passive antenna design is preferred for highest level of robustness. Patch antennas can easily be concealed due to their low profile and conformable structure. This makes it easy to produce patch antennas that are durable and resistant to tough weather conditions. Most patch antennas have service lives of more than 10 years in which they almost never need maintenance while other antennas may rust or wear away due to adverse weather conditions.

1.2.2 High Gain

Another requirement for this type of a system is high gain since the signal needs to be transmitted over a long distance. The antenna determines the range of communication that the system can establish by using the limited amount of power available. A high gain antenna can enable units to communicate over long distances while using a smaller amount of energy. However, obtaining a high gain requires either a larger antenna or an antenna with a narrower beamwidth. (Although the shape and design of the antenna can also affect the gain, increasing its apparent size, these effects are limited.) A very large antenna would be more costly, draw more power and have limited conformability, defeating the purpose of using a patch antenna. Therefore, a directive antenna with a narrower beamwidth should be used but this approach would drastically reduce the coverage area. Several things can be done to overcome this problem and they are explained in the next section. On the other hand the directivity of the designed antenna shouldn’t be too high since that will lead to an extremely narrow beamwidth. When the beamwidth is too narrow, the slightest change in the direction of the antenna will cause the targeted unit to be left

out of the coverage area. In addition to this, two closely placed units may have to be covered by a single wider beam since the beam switching ability of the antenna will not be as flexible as a scanning array. This is to say that the designed antenna cannot possibly have an infinite number of switchable beam positions. Thus, it should have a high gain, but not high enough to require an extremely narrow beamwidth, keeping the gain and beamwidth at optimal values.

1.2.3 Coverage Area (Multiple Beams)

Since the purpose is to enable communication ever long distances, directive beams are required. However, the angle of coverage is very limited with a focused beam. The simplest approach to solve this problem would be using several antennas facing at different locations, but unfortunately this solution will be costly and take a lot of space. The second solution would be using a mechanical system to rotate the antenna. However, this approach would sacrifice mechanical stability, waste energy, require more maintenance and lead to slow switching between targets. In the few seconds required to mechanically rotate the antenna, opportunity to transfer megabytes of essential data will be lost which is unacceptable in most cases. A more complex solution would be the use of scanning beam arrays but these systems are very complicated to design, fabricate and maintain. Therefore, there is a need for a new antenna design that has multiple directive beams that are selectable or can work simultaneously.

In this project, a multibeam antenna design with selectable beams is proposed to enable flexible communication between multiple units at different directions. The multibeam feature will eliminate all disadvantages of the mentioned solutions. The proposed system is a passive array which is most closely comparable to an array

driven by a Butler Matrix [8] or a Rotman Lens [9], [10]. The final design is compared to these systems in Section 4.2.1.

1.2.4 Selection of Transmission Band and Bandwidth

This project aims to develop an antenna that can be used in a wide variety of situations as most applications in today's world require wide bandwidths for high speed data transmission. The 2.45 GHz ISM (Industrial, Scientific and Medical) band, which does not require a license, was chosen as the operating band for the prototype. This frequency is the lowest ISM band available that can handle high speed video and data transmission. A relatively lower frequency, 2.45 GHz, is preferred to increase the range and minimize the effects of small obstacles while keeping costs low since higher frequency hardware have higher costs.

Although a wider bandwidth system than the proposed one is possible, bandwidth was sacrificed for other merits. Because most commercial systems are permitted to only operate in a limited band. For example the 2.45 GHz ISM band, has a bandwidth of 100 MHz from 2.4 to 2.5 GHz. This corresponds to about 4 percent bandwidth.

1.2.5 Efficiency

The designed antenna needs to be efficient since solar powered applications may be used at remote places that don't have access to grid electricity. Also an inefficient antenna will generate more heat and further deteriorate the system performance.

1.2.6 Affordability

Since the goal is to design an alternative to the expensive active arrays that can be used by the general consumer, the antenna needs to be affordable. Therefore, a passive design is adopted utilizing a FR4 substrate which is very affordable and the

most common substrate in the market. Some disadvantages of the thin FR4 substrate are eliminated by the suspended structure which is easy to implement at a low cost. A wider bandwidth design is made possible through the use of the suspended structure and the air gap eliminates the surface wave generation which would otherwise deteriorate the performance in a thick substrate.

1.3 Overview of Patch Antennas

Patch antennas are also called microstrip antennas (MSAs) since they usually consist of a thin sheet of copper placed over a ground plane. This structure is usually formed by using standard or high frequency circuit boards.

1.3.1 History of Patch Antennas

Although the idea of using the microstrip structure as an antenna dates back to 1950's [1], it wasn't until 1970's that MSAs found more practical use [2]. The need for this type of an antenna arose when aircraft, spacecraft and missiles called for a conformal and robust antenna structure that could survive on air vessels [3]. In its early years, MSAs were mostly used in defense and space applications including missiles and spacecraft. High performance active phased arrays were developed to create radars for the defense industry.

1.3.2 Patch Antennas Today

After 1990's MSAs became more popular, since the newly developed devices required smaller and conformable radiators, since most small devices became integrated into wireless networks. It is easy to find MSAs being used anywhere ranging from our computers and multimedia devices to high performance aircraft and satellites. An example of a patch antenna which is embedded in a cell phone can be seen in Figure 5. This figure is an excellent illustration of how small and

conformable patch antennas can be. These features reduce the weight, cost and size of these devices while giving better and wideband communication performance.

Figure 5: An Internal Cell Phone Antenna.

Patch antennas can be easily integrated into printed circuits and even chips. They are also easily grouped together to create arrays by simply joining them with copper traces. The array structure brings another set of benefits including higher gain and beam scanning. For example, almost all of the cellular base stations use patch antennas because they are mechanically more durable and resistant to adverse weather conditions. Some of the other important applications of MSAs' are in RFID (Radio Frequency Identification), RFIC (Radio Frequency Integrated Circuit) and biomedical areas.

A simple patch antenna is shown in Figure 6 with its protective coverage illustrating how easily a patch antenna is concealed from adverse environmental effects. Next to this antenna is an internal view of a 4-element MSA array. It is seen here that the feeds to the elements are at equal length; this type of a structure is usually used when the gain of a single element is not sufficient.

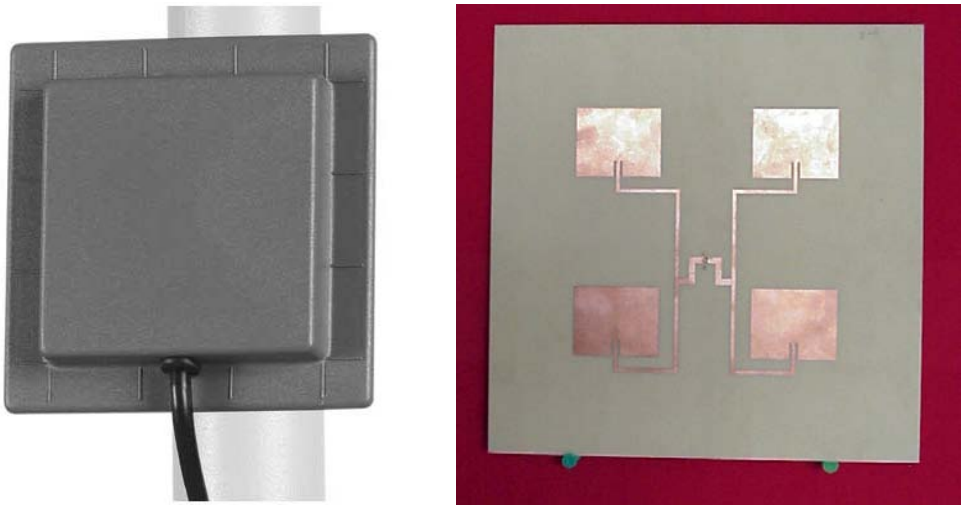

Figure 6: A MSA in its commercial cover and a uniformly fed 4-element array.

1.3.3 Advantages and Disadvantages of Microstrip Antennas

Microstrip antennas have several significant advantages over conventional antennas, so they are used in a broad range of applications where frequencies range from 100MHz to 50GHz and sometimes even higher. However, microstrip antennas also have some disadvantages compared to conventional antennas. Some major advantages and disadvantages of MSAs are as listed in Table 1.

Table 1: Advantages and disadvantages of patch antennas.

Advantages	**Disadvantages**
Low profile: small volume, can be miniaturized	Narrow bandwidth
Light weight	Low radiation efficiency
Conformable	Poor power capability
Low cost: easily fabricated, affordable materials	Limited antenna gain
Linear and circular polarizations are possible with simple changes in the feed position	Possibility of excitation of surface waves
Multiple band designs can be made	Poor polarization purity
Easy integration with other circuits and solid state devices	Poor isolation between the feed and the radiating elements
Design Versatility	Poor scan performance
Feed lines and matching networks are fabricated along with the antenna structure.	Sensitive to fabrication errors

It is possible, to avoid some of the disadvantages by using appropriate designs. For example, use of a thicker substrate increases bandwidth and gain, a low permittivity substrate reduces surface waves and array configurations may be used to enable beam shaping and beam steering.

A comparison between several types of antennas is presented in Table 2. Although patch antennas don't possess the best properties in all fields, they have some unique features that cannot be obtained using other types of antennas. The most important feature of MSAs is their conformability which allows them to be implemented in small electronic devices.

Table 2: Comparison of properties of some antenna types.

Antenna Type	Typical Gain	Conformability	Size	Mechanical Stability	Interface Compatibility	Cost
Patch	3-8 dB	Very good	Small	Very good	Very good	Low
Dish	>10 dB	Bad	Large	Bad	Bad	High
Dipole	1.7 dB	Good	Small	Bad	Average	Low
Yagi-Uda	5-15 dB	Bad	Large	Bad	Bad	High
Horn	10-20 dB	Bad	Med	Average	Bad	High

Chapter 2

THEORETICAL DESIGN

2.1 Transmission Line Model

The transmission line theory is used to analyze characteristics of microstrip lines at high frequencies [3]. The basic understanding about how MSAs radiate can also be gained through analyzing them using the transmission line theory. Although this method is relatively inaccurate, it is one of the easiest antenna models that can be used to explain the operating principles of MSAs. In this model, a MSA is viewed as a resonant section of a low impedance microstrip transmission line. So it may be treated as a matching network that matches a standard 50 Ω transmission line to the wave impedance of the free space which is 377 Ω.

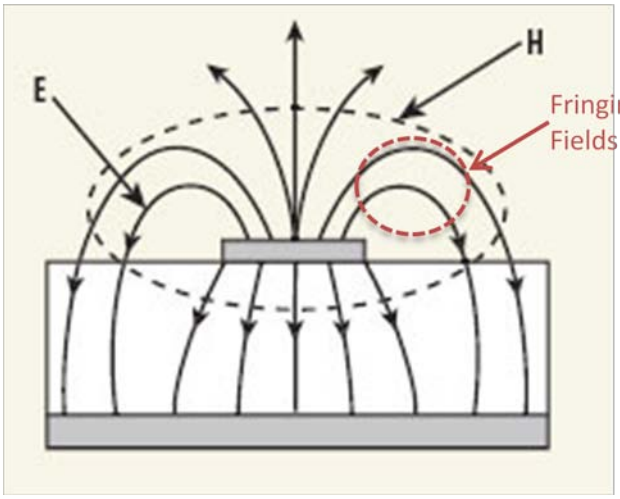

Figure 7: The electric and magnetic fields in a microstrip structure.

2.1.1 Fringing Effects

Fringing fields are the electromagnetic fields that leak outside of the area that is between the microstrip and the ground (see Figure 7). The amount of fringing depends on the dimensions of the patch, substrate height and dielectric constant. While these fields are negligible in a thin microstrip that is close to the ground, they become more significant as the lines become wider causing them to perform as antennas. Because of the fringing effects, the MSA electrically appears greater than its physical dimensions. This model is used in section 2.2 to design a rectangular patch antenna and the designed antenna's simulation results are presented in section 3.2.

2.2 Rectangular Patch

In this section, the procedure for manually designing a rectangular microstrip patch antenna (see Figure 8) is explained and calculations are made to determine the dimensions of a patch working at 2.45 GHz ISM band. While different designs and feed structures will be presented in the following chapters, no detailed theoretical design procedures are presented due to the complexity of the required calculations. It is almost impossible to determine all of the radiation characteristics of antennas doing calculations by hand. Therefore, electromagnetic simulation software packages are utilized for the analysis.

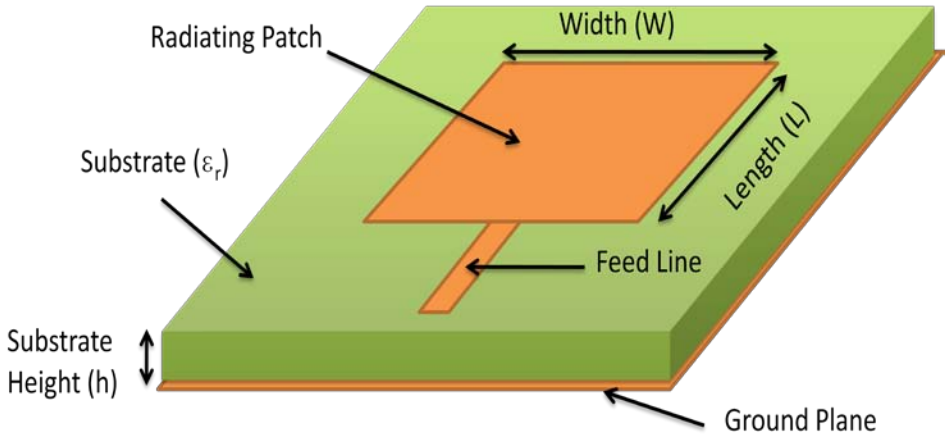

Figure 8: A typical rectangular patch geometry.

2.2.1 Design Parameters

Before a patch antenna can be designed some essential parameters need to be established. First, the resonant frequency (f_o) must be chosen appropriately which is 2.45 GHz in this particular case. Next, the dielectric constant (ε_r) of the substrate that the patch will be printed on should be determined. For this project a FR-4 substrate (see appendix B) is used which has a dielectric constant of 4.4 (approximately[1]). Lastly, the height of the dielectric substrate (h) should be known. The height that was used in this project was 1.57 mm which is the standard FR-4 board thickness.

2.2.2 Design Procedure and Calculations

This procedure will explain the steps needed to be followed in order to calculate the width (W) and the resonant length (L) of the patch when given the specifications mentioned in the previous section (f_o, ε_r and h). The antenna designed in this section is simulated in FEKO and results are presented in section 3.2. The transmission line model is utilized in order to make these calculations [3].

[1] The permittivity of a FR-4 substrate may vary between 4.2 and 4.8 due to differences in production methods. Since FR-4 is not designed as a high frequency substrate, permittivity values at high frequencies are usually not supplied by the manufacturers.

Step 1: Calculation of the Width (W): The width of the antenna can be calculated using Equation 5. The width affects the input impedance of the antenna much more than it affects the resonant frequency.

Substituting c = $300x10^9$ mm/s, $\varepsilon_r = 4.4$, and $f_o = 2.45$ GHz; we get: **W = 37.26 mm**

Step 2: Calculation of the Effective Dielectric Constant (ε_{reff}): Since some of the field goes through the air to reach the ground plane, the permittivity will seem smaller than it actually is. Equation 6 gives the effective dielectric constant which takes into account the fringing effects as:

Substituting $\varepsilon_r = 4.4$, W = 37.26 and h = 1.57 mm; we get: **ε_{reff} = 4.085**

Step 3: Calculation of the Effective Length (L_{eff}): The length is the main parameter that affects the resonant frequency of the patch. This is the apparent electrical length of the patch which is slightly larger than the actual length due to fringing effects. Equation 7 gives the effective length of the patch antenna which uses the effective dielectric constant to considers the effects of the fringing as:

Substituting ε_{reff} = 4.085, c = 300x10^9 mm/s and f_o = 2.45 GHz; we get: **L_{eff} = 30.29 mm**

Step 4: Calculation of the length extension (ΔL): This is the difference between the real length and the apparent length. Equation 8 gives the length extension as:

$$\frac{\quad}{\quad}$$

Substituting ε_{reff} = 4.085, W = 37.26 and h = 1.57 mm; we get: **ΔL = 0.269 mm**

Step 5: Calculation of the actual length of the patch (L): The actual length can be obtained using Equation 9. Here the extension from each side must be deducted from the effective length in order to obtain the actual length required to resonate this patch at 2.45 GHz.

Substituting L_{eff} = 30.29 mm and ΔL = 0.269 mm; we get: **L = 29.75 mm**

Step 6: Calculation of the ground plane dimensions (L_g and W_g): The transmission line model assumes an infinite ground plane. However, for practical reasons the ground plane needs to be finite but at the same time it must be big enough to act like an infinite ground plane so that the transmission line model is still valid. It has been shown that a ground plane that has an extra perimeter of about six times the substrate height is large enough to imitate an infinite ground plane.

Therefore, Equations 10 and 11 can be used to calculate the minimum size of the ground plane that should be used.

Substituting L = 29.75 mm, W = 37.26 and *h* = 1.57 mm; we get: **L_g = 39.17 and W_g = 46.68**

2.3 Equilateral Triangular Patch Design

The theoretical design procedure for an equilateral triangular patch is explained in this section. The design parameters of this antenna are similar to the rectangular patch as explained in section 2.2.1. The difference here is the use of side length (S) instead of the width and the length.

2.3.1 Design Procedure and Calculations

A standard formula [11] for calculating the resonance frequency of an equilateral triangular patch for different modes is given in Equation 12. This formula is derived using the "Cavity Model" which treats a microstrip as a waveguide where certain modes can propagate through. This is an alternative model to the transmission line model and its details are outside the scope of this thesis.

Substituting *f* = 2.45 Ghz, c = 300x109, m =1, n=1 and ε_r = 4.4; we get ***S* = 38.9 mm.**

When ε_r = 2; we get ***S* = 57.7 mm.**

Although this formula can't give accurate results for antennas using suspended substrate structures with large heights, it can be used as a starting point. Then, the calculated value of the side length can be modified in FEKO simulations to obtain the right resonance frequency.

A more accurate calculation can be made using a modified version of Equation 12, which accounts for the air gap. This method is shown to be accurate for
[11], [12], [13].

2.4 Array Theory and its Effects

Arrays of MSAs are very common since they are very easily interfaced together. The antenna designed in this thesis also utilizes an array configuration; therefore, it is important to understand the basic array theory and the effects of array configurations/phase shifts.

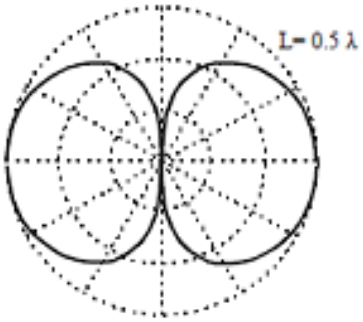

Figure 9: Radiation pattern of a standard λ/2 long dipole antenna.

Figure 9 shows the radiation pattern of a standard dipole antenna which is used in an array configuration in Figure 10. This figure shows phase/array effects, where parallel dipoles are viewed in a perpendicular position from the top. Varying the phase difference between the array elements causes a change in the radiation pattern. The phase can be varied electronically or by using fixed phase shifters. This type of

steering eliminates the need for mechanically rotating the antenna. Another array effect is the increase in directivity when more elements are used.

The radiation pattern of an array varies considerably with frequency due to the frequency sensitivity of the phase shifting networks and apparent change in element spacing which is measured in wavelengths. However, these effects will not be very significant for the relatively narrow 100 MHz range of interest between 2.4 and 2.5 GHz.

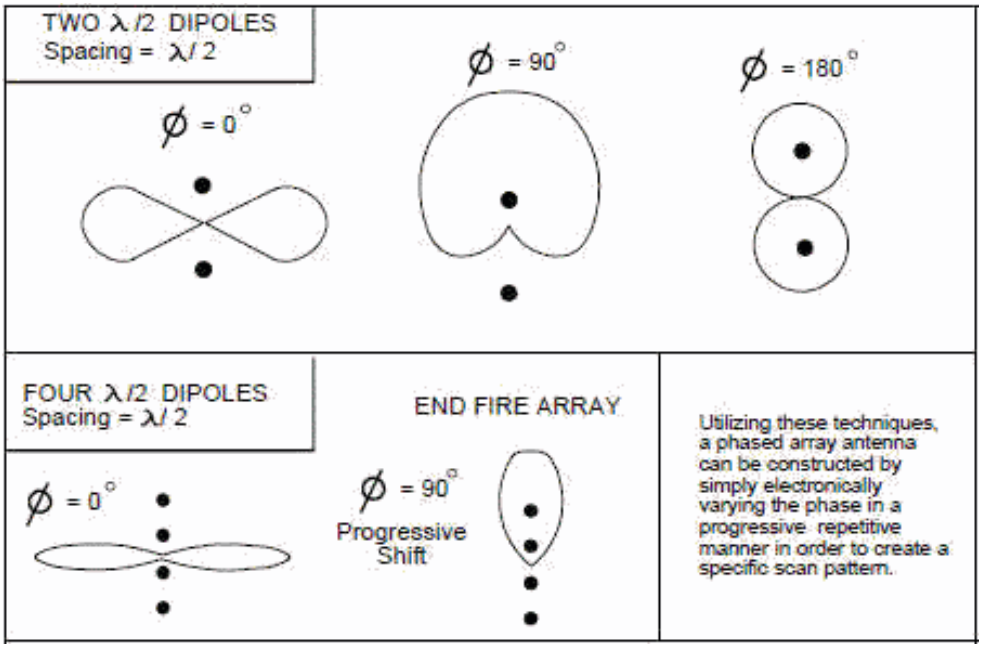

Figure 10: The effects of phase and array configuration on the radiation pattern of a standard /2 long dipole antenna [6].

Although there are many kinds of array configurations, there are especially two kinds of configurations that are relevant to the work done in this thesis. The first is the linear phased array which is a good basis for explaining introductory array theory and could be created by using a Butler Matrix [8]. The second configuration is the Rotman Lens [9], [10] driven array, which is another passive array configuration.

2.4.1 Linear Phased Array

The linear array is the easiest configuration to analyze and it forms the basis for most array designs. The direction and shape of the beam radiated by the array can be adjusted by controlling the phase and amplitude of excitation to each element. Figure 11 schematically illustrates a linear array with element spacing "d" and a phase shift of "phi (Φ)" which cause a steering angle of "theta (θ)".

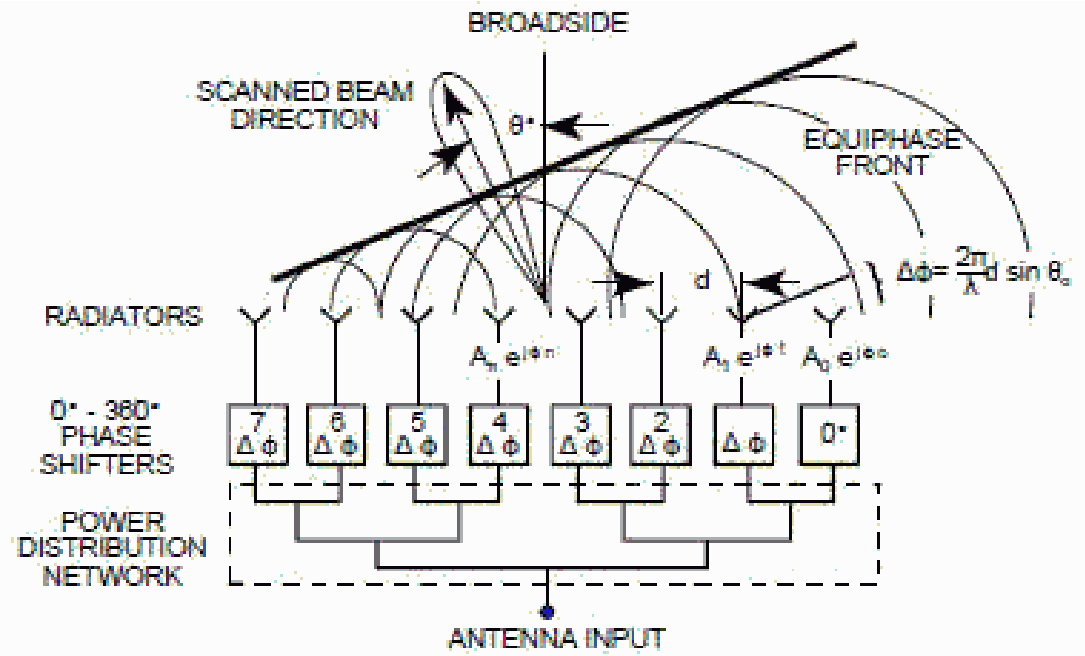

Figure 11: Linear antenna array showing the phase shifters and the shift in the direction of radiation through addition and cancellation of beams [6].

Feeding all the antennas with the same phase will produce a broadside beam which is perpendicular to the surface in the case of a MSA. Steering the beam to other angles requires the phase shift (ΔΦ) to be adjusted. The phase shift required to achieve a certain steering angle (θ) can be determined by Equation 13.

A linear phased array can radiate a beam in any angle as the formula indicates; however, the scan angle is limited by the beamwidth of the array elements. It should also be noted that this antenna can only scan in one dimension; an array with two-dimensional element placement is required to scan in two dimensions. Beam shape and side lobe levels can be tuned further by varying the power received at each element but this topic is out of the scope of this thesis.

The mutual coupling between the elements is also an important phenomenon that affects matching and beam patterns. This is the main reason why the initial array design in section 3.5.3 had to be modified in section 3.5.4 after each individually designed part was put in place.

2.4.2 Butler Matrix

Linear arrays can be fed by the Butler Matrix [8], which is a kind of a feed network that provides a fixed phase shift between the elements that can be changed depending on the chosen input terminal. It has multiple input ports and fixed phase shifts created via lengths of microstrip lines. This network is especially important since it is comparable to the novel circular feed network proposed in this thesis.

A Butler Matrix requires four branch line couplers and two crossovers. These components take space, increase the costs and introduce more losses. Another disadvantage of this network is its inability to steer beams in more than one dimension since it can only control linear arrays.

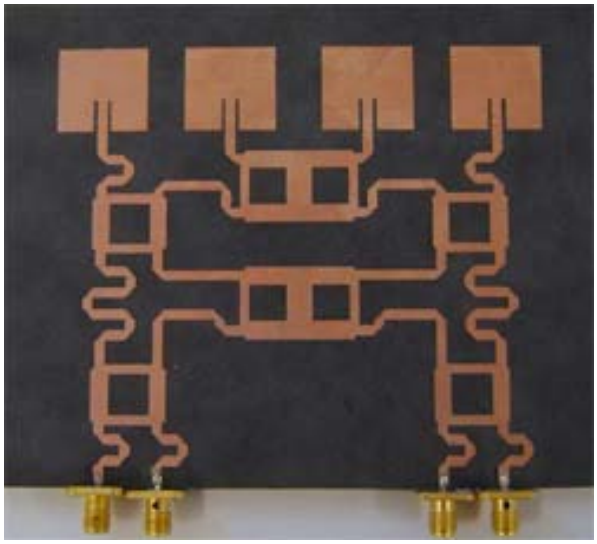

Figure 12: A Butler Matrix with 4 input ports feeding 4 rectangular elements of a linear array [14].

2.4.3 Rotman Bootlace Lens

Another passive device used to feed arrays is the Rotman Bootlace type Lens [9], [10] shown in Figure 13, as it was originally drawn in the patent. A physical Rotman Lens is shown in Figure 14. This device is composed of a lens shaped body and ports that surround it. The principle of operation is very similar to the novel structure proposed in this thesis; it also utilizes the distance between the feed point and the output ports creating a successive phase delay.

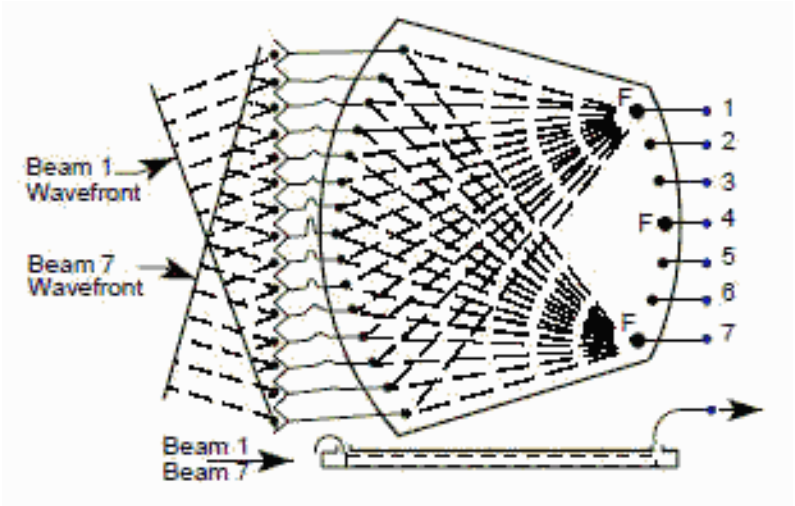

Figure 13: Rotman Bootlace Lens geometry from the original patent by W. Rotman [9].

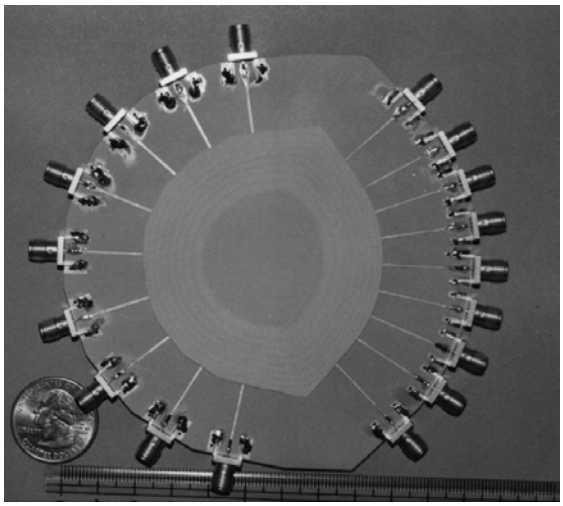

Figure 14: A physical Rotman Lens geometry [15].

Chapter 3

SIMULATION AND DESIGN

3.1 Overview of the Utilized Software Packages

3.1.1 ADS

This software, by Agilent, is mainly used for high frequency circuit design and digital signal processing. ADS [16] stands for “Advanced Design System”. ADS makes use of two solvers. One of them uses the MoM (method of moments) to make electromagnetic analysis and the other is used to analyze schematics. The EM solver can only handle planar structures. The schematic designer can be used to analyze Analog/RF networks or Digital Signal Processing networks.

The schematic designer allows fast design and tuning of microstrip circuits and it was used in Analog/RF mode to design the circular feed network. This design is presented in section 3.4.1.

3.1.2 FEKO

This software suite [17] can be used to solve a wide range of electromagnetic problems including EMC analysis, microwave circuit design and scattering analysis in addition to antenna design. FEKO is a German abbreviation that stands for “field computations involving bodies of arbitrary shape”. FEKO mainly uses hybrid MoM (method of moments) but it also allows the use of some other methods such as UTD (uniform theory of diffraction), GO (geometrical optics), PO (physical optics), FEM (finite element method) and MLFMM (multilevel fast multipole method) [18].

3.2 Simple Rectangular Pin Fed Patch

The rectangular patch antenna designed in section 2.1.2 is modeled and simulated using FEKO electromagnetic analysis software. The antenna model can be seen in Figure 15 where conductive areas are shown in the center and the dielectric material is shown as a cuboid underneath the conducting patch. The bottom face of the cuboid was defined as a conductor to model the ground plane. The model is shown with the mesh grid applied to it. The mesh size was chosen to be less than one twentieth of the free space wavelength in order to accurately model the geometry.

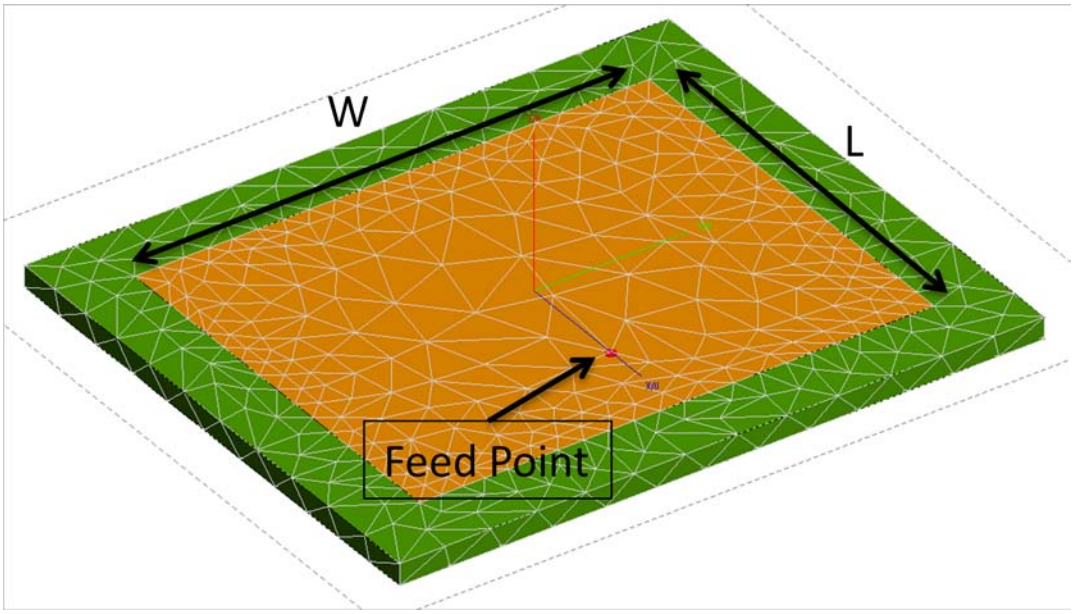

Figure 15: Rectangular microstrip patch.

An ideal pin feed with a voltage source is used in this initial model. The feed is located 7 mm from the center of the patch in the direction of the resonant length. The location of the feed was chosen after testing with a few different points. The feed point determines the input impedance of the antenna which has to be optimized for best resonance and minimum loss. The input impedance of the simulated antenna, seen through the pin port, is given in Figure 16. The real component of the impedance has the higher peak value and the other line represents the imaginary component.

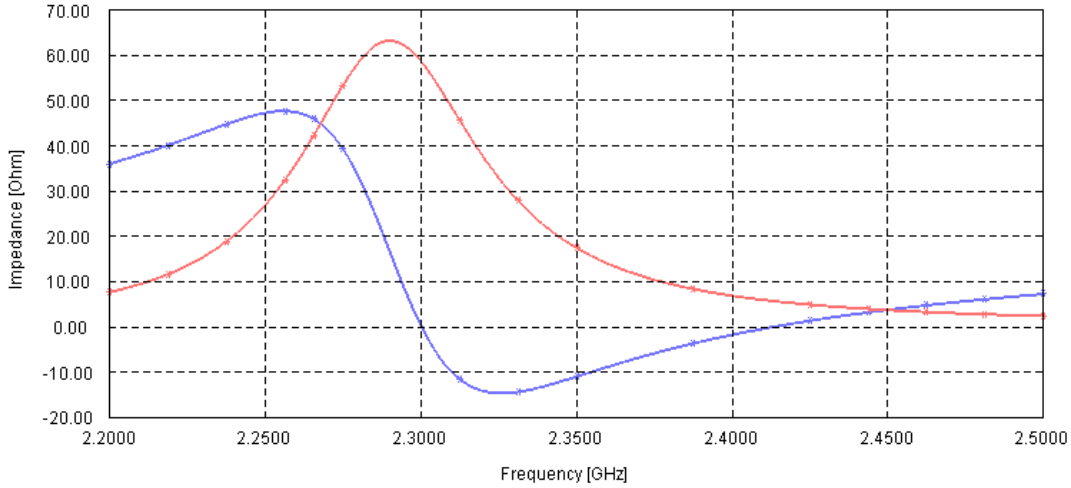

Figure 16: Input impedance of the pin fed rectangular patch.

The Reflection Coefficient (S_{11}) of the antenna is illustrated in Figure 17, where two important parameters can be revealed. Firstly, a resonance is observed at 2.31 GHz which is the point with the lowest amount of reflection. There is about 140 MHz of deviation from the calculated results in section 2.1.2. This deviation was expected since the design formulas are not perfectly accurate; however, it is beyond the tolerable limits for a practical system. At this point, advanced electromagnetic simulation software can be utilized to quickly fine tune the antenna design. Secondly, the bandwidth of the antenna can be measured which turns out to be around 51 MHz. This corresponds to 2.2 percent bandwidth which is a typical value for a simple and unmodified patch design with a thin substrate.

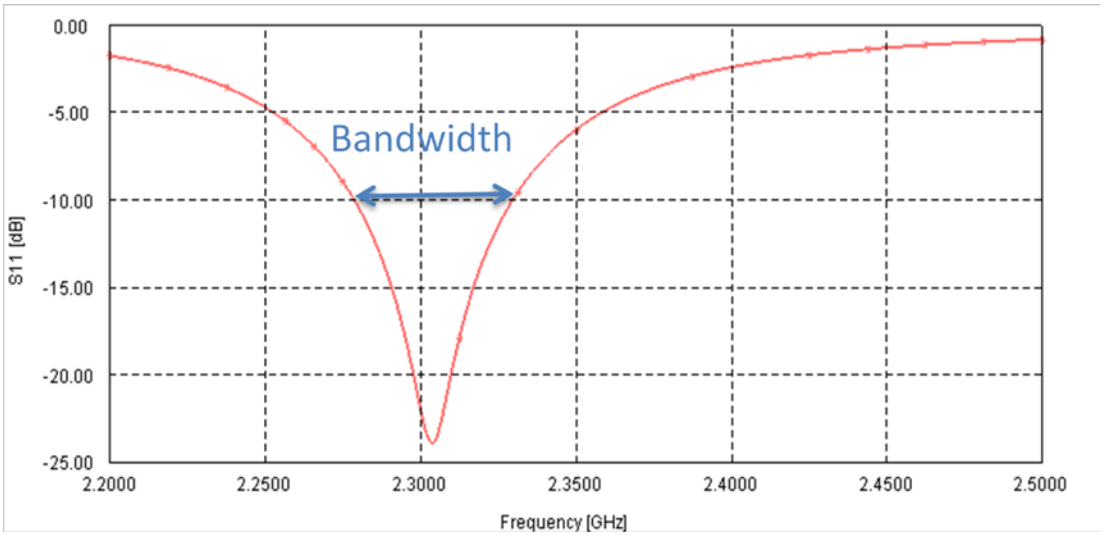

Figure 17: Input reflection coefficient and the bandwidth of the pin fed rectangular patch.

Figure 18 gives the three-dimensional radiation pattern of the antenna, which indicates a maximum gain of 2.9 dB.

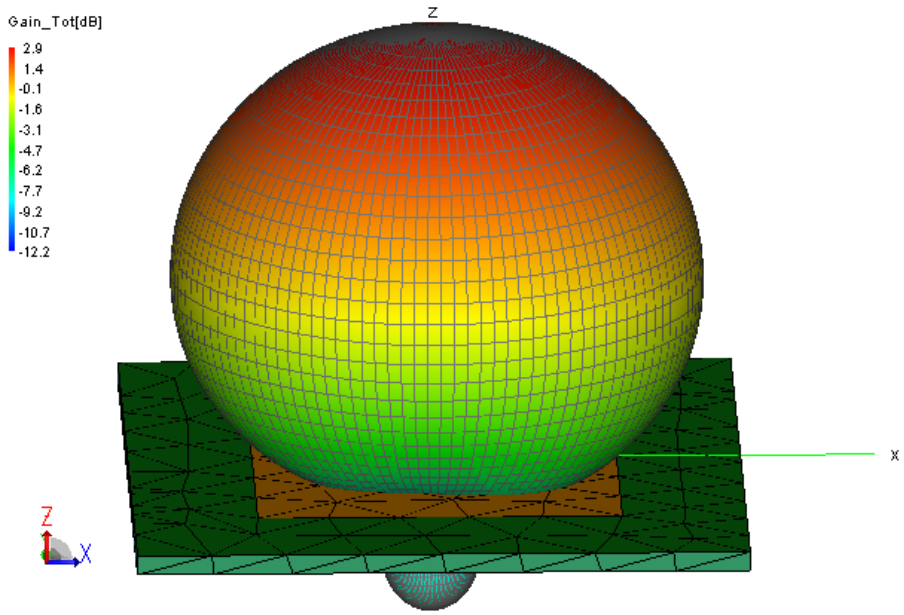

Figure 18: 3-D radiation pattern of the rectangular pin-fed patch.

Figure 19 shows a cut plane of the radiation pattern. The beamwidth can be read more easily from this figure which is measured at 3 dB down from the peak. So the

beamwidth covers the range of angles where the gain is larger than about 0 dB for this case. The beamwidth of this antenna is about 100 degrees.

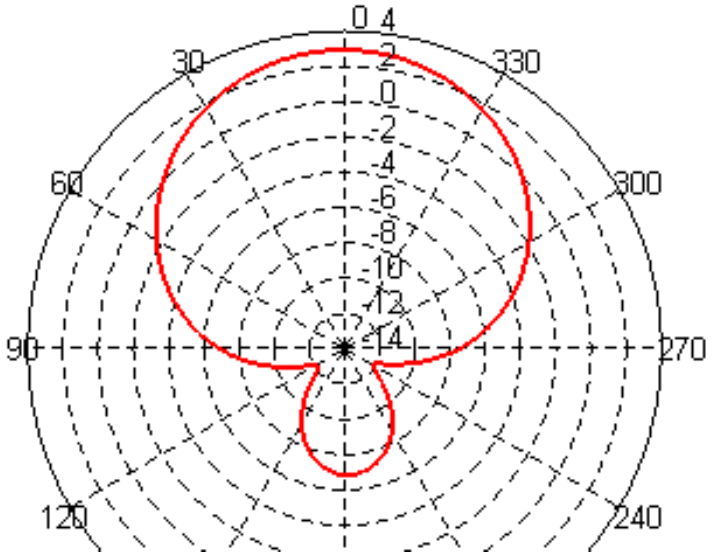

Figure 19: A cut-plane of the radiation pattern of the rectangular MSA.

3.3 Triangular Antenna Design

In this section, simulation results of a triangular MSA design are presented. Final array elements will be based on this design. The triangular shape is chosen since it is suitable for creating a circular array with uniform distances between the element edges. This MSA is designed with a microstrip feed so that it can easily be interfaced with the circular feed network. A λ/4 impedance transformer is used in order to match the antenna to the 50 Ω feed line. However, this feed structure and some other parts of this antenna will require further modifications in the combined array structure. This is mostly due to the coupling effects between the antennas and the perfect 50 Ω port model used to simulate this antenna. This design is a relatively simple model that doesn't have any modifications to improve the bandwidth or gain. The triangular MSA geometry can be seen in Figure 20 with the applied mesh.

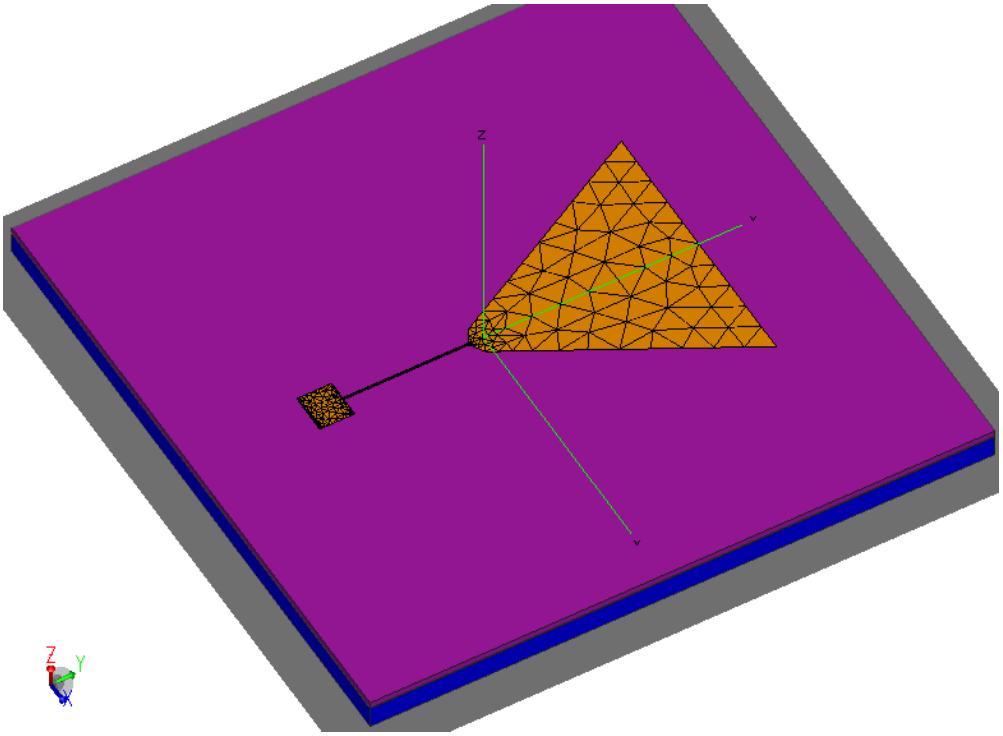

Figure 20: Equilateral triangular MSA geometry.

The antenna is an equilateral triangle with sides of length 54 mm except for the small modification made around the feed corner. The λ/4 transformer is 25mm long and 0.4 mm thick. The antenna is placed on a 1.57 mm thick FR-4 substrate which is suspended by 5 mm over the ground plane. This substrate structure increases the gain and bandwidth of the antenna. The impedance bandwidth of the antenna can be obtained from the input reflection coefficient graph given in Figure 21. The patch resonates at 2.456 GHz and the bandwidth ranges from 2.423 to 2.492 GHz. So the total bandwidth is 69 MHz which is equivalent to about 2.8 percent.

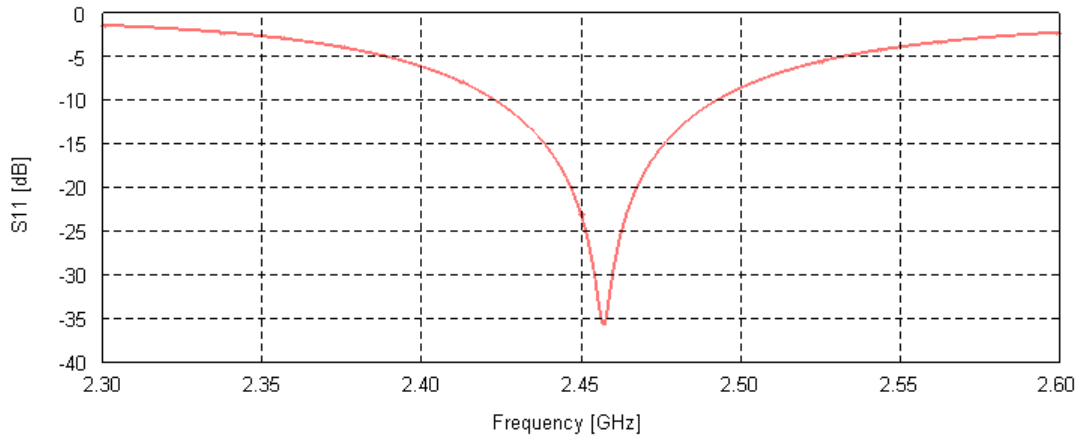

Figure 21: Triangular antenna S11 performance results (FEKO).

The radiation pattern of the antenna, as seen in Figure 23, is very uniform with a half power beamwidth of more than 90 degrees which is very suitable for array use. This means that the array elements will be losing 3 dB of power after they are 45 degrees of the center. The gain of the antenna was found to be around 8 dB; however, this value is expected to be slightly lower in practice since the use of an infinite ground limits the losses.

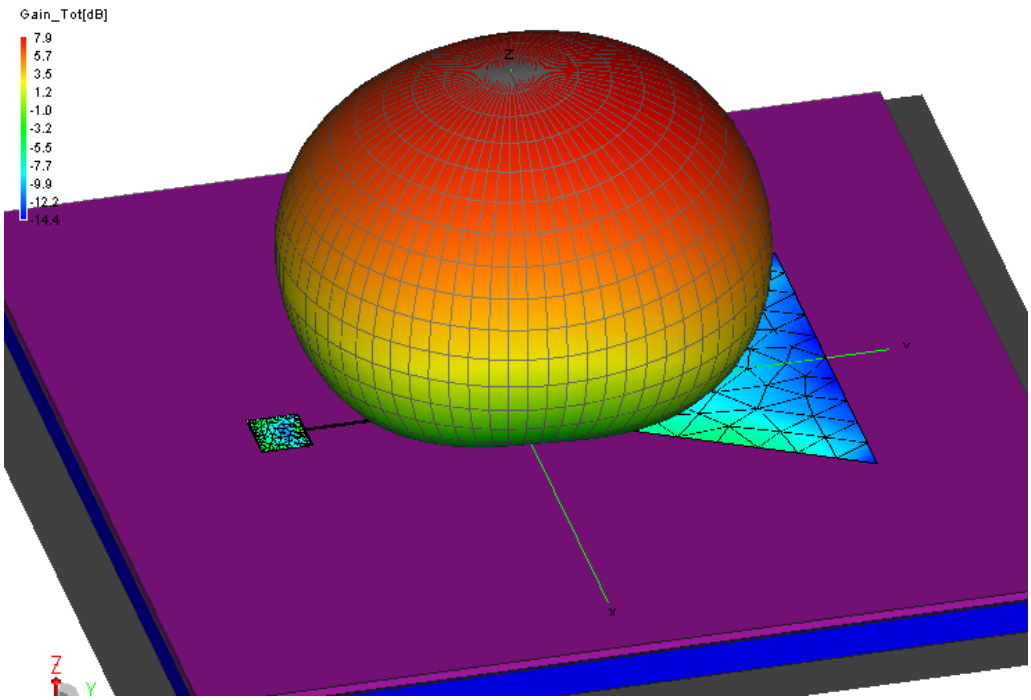

Figure 22: 3-D radiation pattern of the equilateral triangular MSA.

No back lobes are present since an infinite ground plane is used. The small difference of the pattern in the two cut planes, shown in Figure 23, is due to the asymmetry introduced by the feed structure.

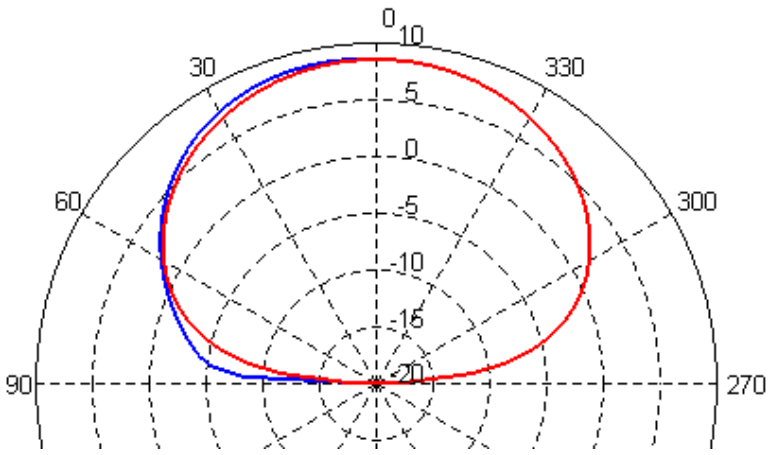

Figure 23: Radiation pattern of the triangular MSA (plotted for $\Phi = 0^o$ and $\Phi = 90^o$)

3.4 Circular Feed Network Design

A novel feed network structure for circular MSA arrays is presented here with simulation results from two different software packages. The feed network is unique since it delivers equal power to all elements of the array with different phases depending on the feed location.

The circular feed network was first deigned in ADS and later modeled in FEKO for a more accurate analysis. The circular divider should distribute the power equally between the antennas but create a delay to feed each port with a different phase, leading to the beam steering effect.

The divider was designed on a multilayer substrate composed of 1.57 mm FR4 and 5 mm layer of air followed by the ground plane which is the same substrate that is used for the radiating elements. Although this configuration has higher losses, having the

divider and the MSAs on the same substrate will avoid discontinuities and simplify the production process, reducing the cost.

3.4.1 Circular Divider Design using ADS

The divider was modeled as an ADS schematic using microstrip models such as bends, straight lines and tee junctions. 60-degree corners were used to model the round divider since curved microstrip models were unavailable for multilayer substrate configurations. The divider terminals were terminated with 50 Ohm loads for the S-parameter analysis. The simulation of this circuit took less than few seconds, allowing fast tuning of many parameters using the tuning wizard in ADS which is shown in Figure 24. Many parameters can be varied using the tuning wizard including the microstrip dimensions, the dielectric constant and height of the substrate. The schematic can be seen in Figure 25 where "S_PARAMETERS" module defines the simulation parameters, "VAR" module defines the variables used for tuning and "MLSUBSTRATE3" module is used to define a 3 layer substrate.

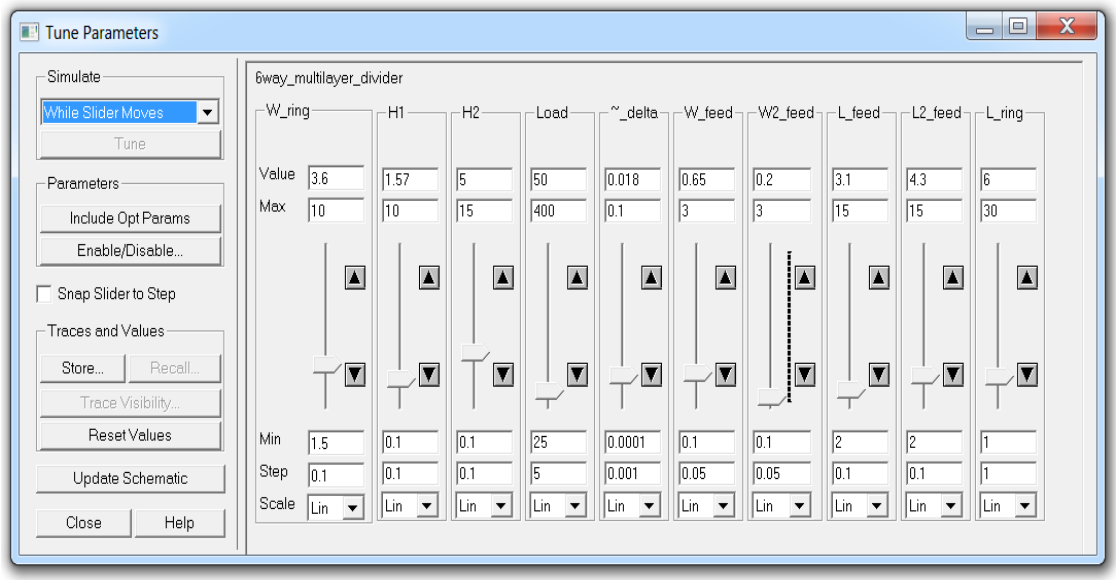

Figure 24: Tuning wizard in ADS.

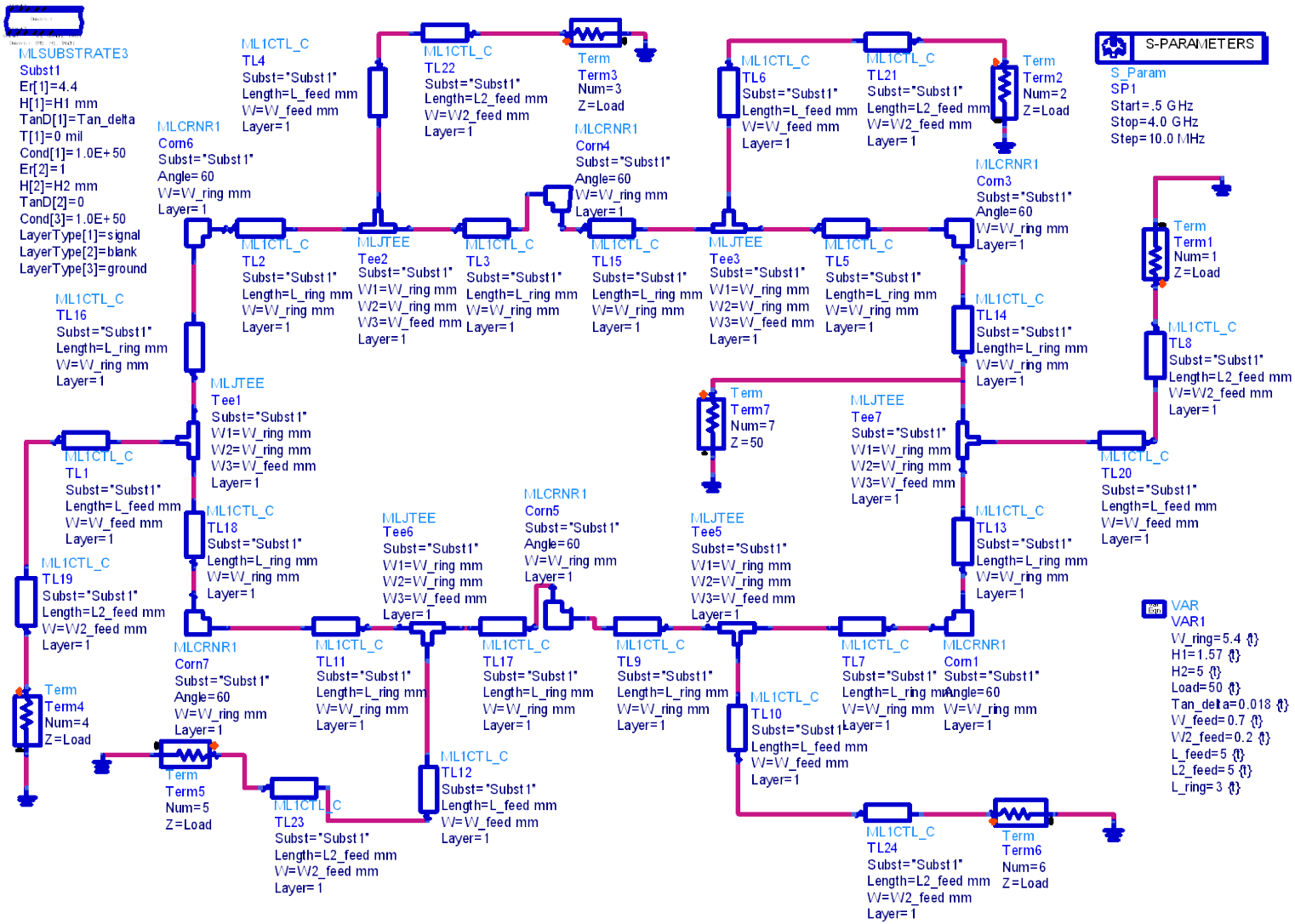

Figure 25: Circular feed network schematic generated using multilayer microstrip models of bends, tee junctions and straight lines in ADS.

Figure 26 shows a graphical representation of the circuit layout which is generated automatically in ADS using the schematic design in Figure 25. ADS can also carry out EM simulations of planar structures like this one but this function was not used since FEKO can be used to get more accurate and detailed results. This simulation is presented in the next section.

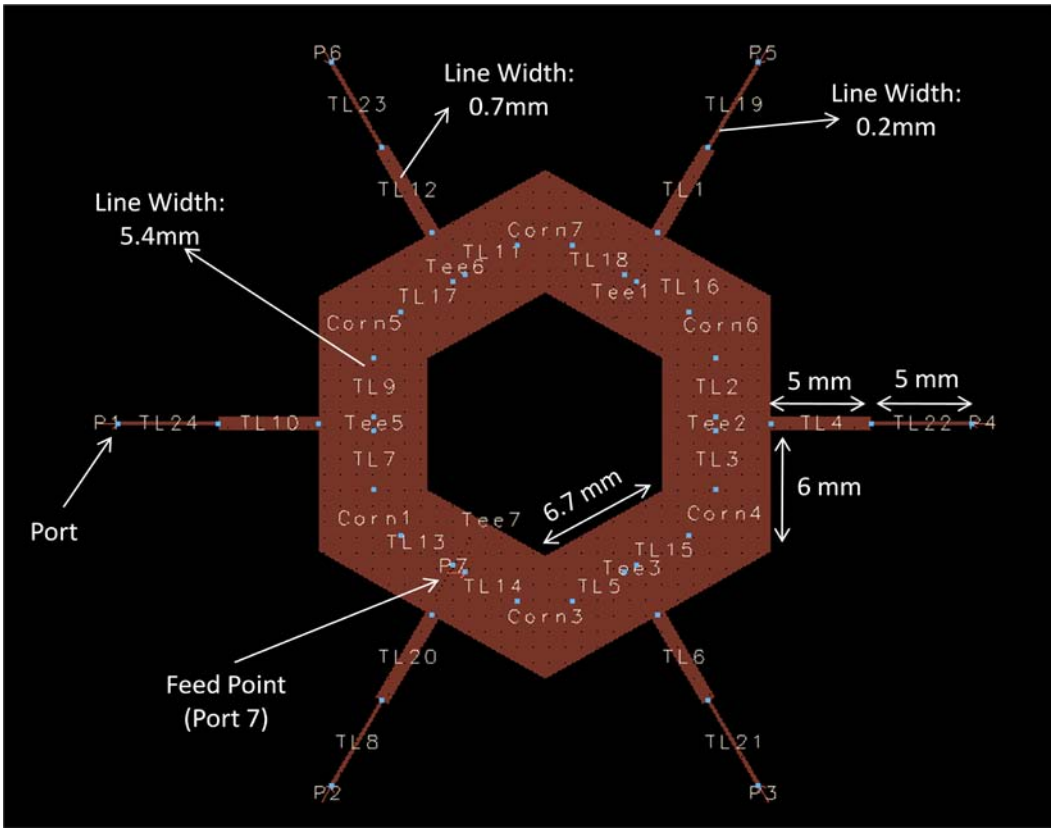

Figure 26: Circular feed network layout generated using the schematic model in ADS and its dimensions as shown.

Figure 27 through 29 give the simulation results of the final circuit. In Figure 27, input reflection coefficient (S11) is presented in dB scale. From this figure we can see that the -10 dB bandwidth is more than 810 MHz, ranging from 2.24 to 3.05 GHz as marked by “m8” and “m9”. When the band of interest (2.4-2.5 GHz) is examined, it is seen that the S11 is below 12.99 dB as indicated by markers “m10” and “m11”.

This S11 value indicates that the maximum reflected power is less than one twentieth of the input power within the band of interest.

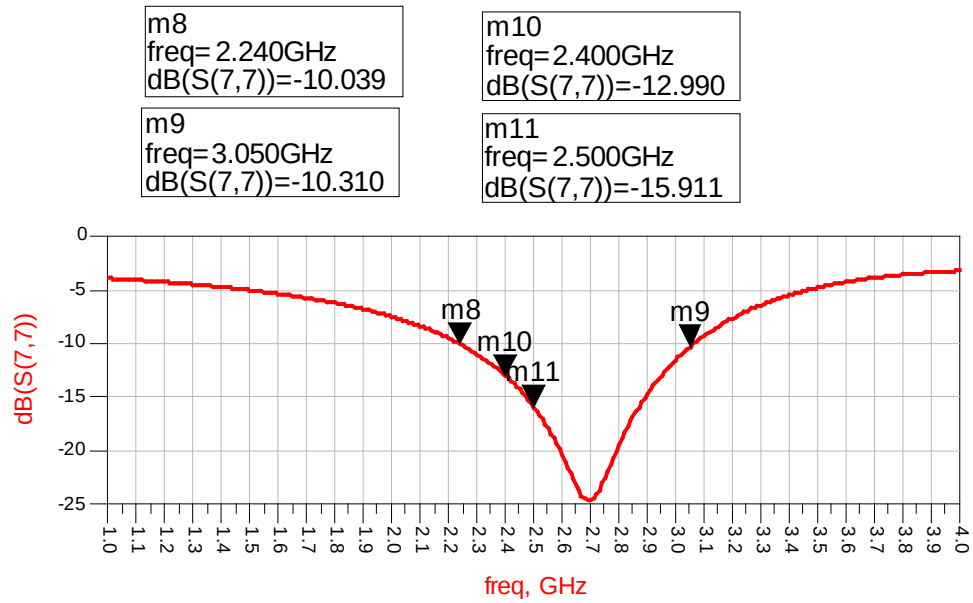

Figure 27: Circular feed network input reflection coefficient (S11) results from ADS.

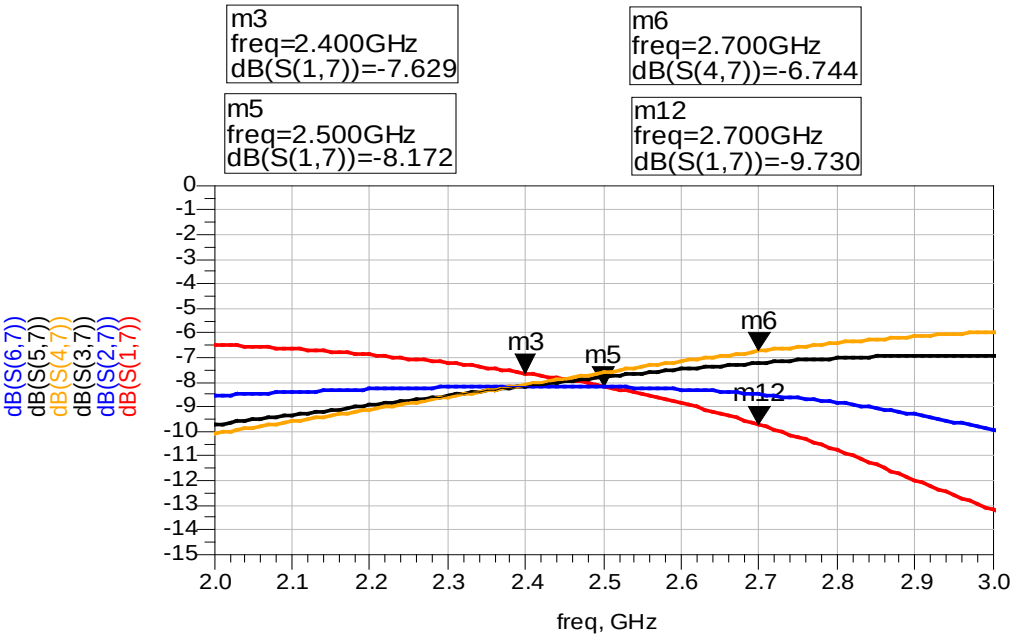

Figure 28: Circular feed network output power level variations as computed in ADS, which shows what portion of the input power is transmitted to output terminals.

The graph in Figure 28 shows the transmitted power from the input (port 7) to the six other branches that will feed the MSAs. Note that only 4 lines are visible although 6 were plotted. This is due to the overlap of S13 with S15 and S12 with S16 because these ports are symmetrical. The maximum variation of the power output between the ports is about 0.45 dB between 2.4 and 2.5 GHz (see markers 3 and 5). The variation is less than 3 dB in the range from 2.1 to 2.7 GHz. The average power level at the output ports is about -8dB relative to the input power. This level indicates that each of the six ports receives about 15.8 percent of the input power and the remaining 5 percent is the reflection loss as seen in Figure 27. A simple calculation will show that 100 percent of the power is present at the ports, which means that this simulation doesn't take the radiation losses into account. These should be a noticeable amount of loss due to radiation especially due to the thick substrate used. The FEKO simulation, presented in the next section, incorporates these losses.

Unlike the power, phase of the signal needs to vary between the ports to create the beam steering effect. The phase plots of the output signals are illustrated in Figure 29. The difference between ports 1 and 2 is about 20 degrees; between ports 2 and 3 is about 13 degrees and between ports 3 and 4 is 4 degrees. Although the phase of each port is linear with respect to the frequency, the variation of phase between the ports is not. Effects of this behavior can only be understood when the complete array is simulated.

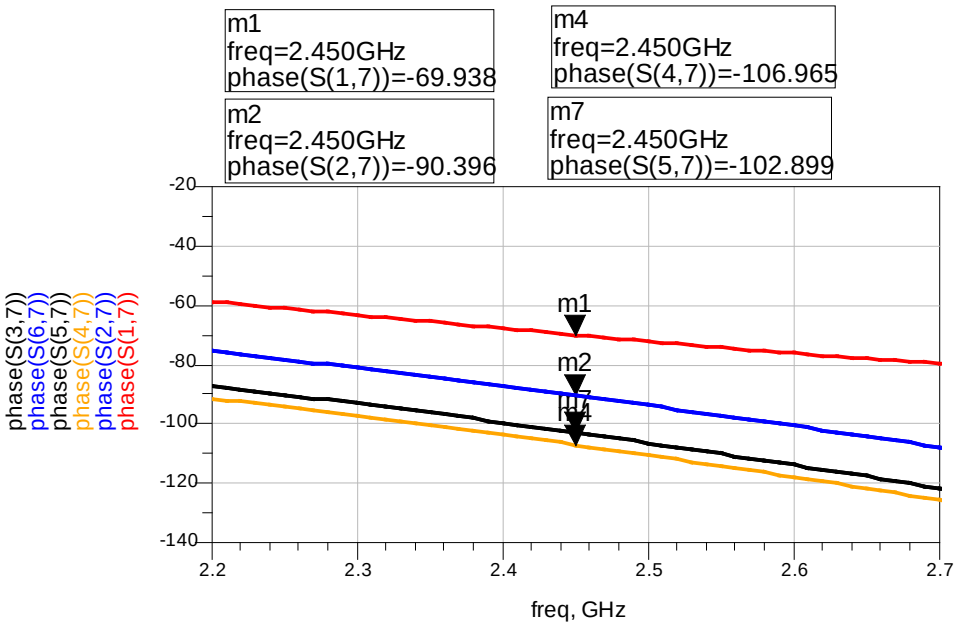

Figure 29: Circular feed network phase angles measured at the output ports using ADS.

3.4.2 Circular Feed Network Design using FEKO

The circular feed network is modeled and simulated in FEKO. A comparison of ADS and FEKO results are presented along with the final design. However, this design will be fine tuned after all elements are connected together.

3.4.2.1 Comparison of FEKO Feed Network model with the ADS model

The divider body was modeled with a circular geometry in FEKO, without the corners that had to be used in the ADS model. The geometric model of the divider can be seen in Figure 30. The initial parameters were taken directly from the ADS model where the circle has a diameter of 25 mm and the center cutout has a diameter of 14 mm. A tab extending towards the center of the circle was created to place the input port but the rest of the model was kept the same. The tab dimensions are 2.5 mm wide by 1.9 mm long. The ground was modeled as an infinite plane in this simulation due to computational limitations.

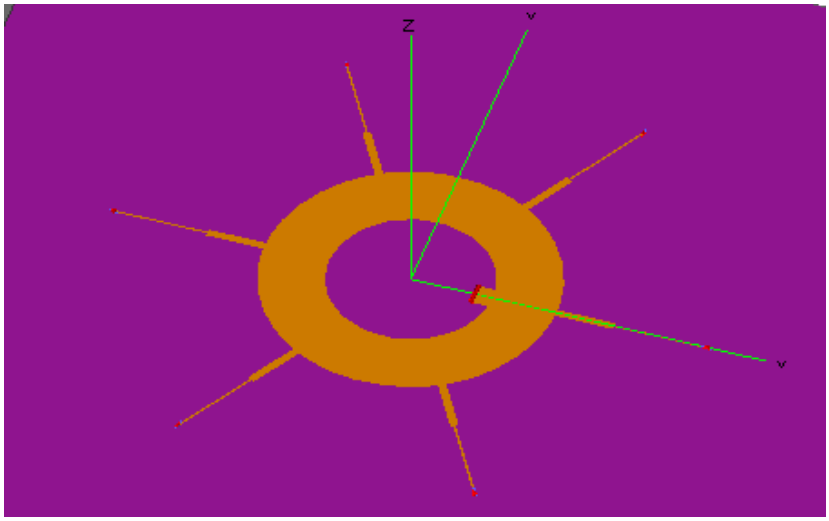

Figure 30: Circular divider geometry in FEKO.

The input reflection coefficient (S11) of the feed network simulated in FEKO can be seen in Figure 31. The network seems to reach the best matching at around 2.7 GHz, which is the same as the ADS results. However, the minimum S11 is at -13.5 dB instead of the -25 dB reached in ADS. The impedance bandwidth of this model is 1.2 GHz ranging from approximately 2.1 to 3.3 GHz but the bandwidth was found to be 0.8 GHz in ADS. So it seems like the slight change in the feed structure caused a tradeoff between S11 and bandwidth. On the other hand, the behavior in the band of interest (2.4 to 2.5 GHz) stays almost the same with an S11 of -11.5 dB at 2.4 GHz and -12 dB at 2.5 GHz.

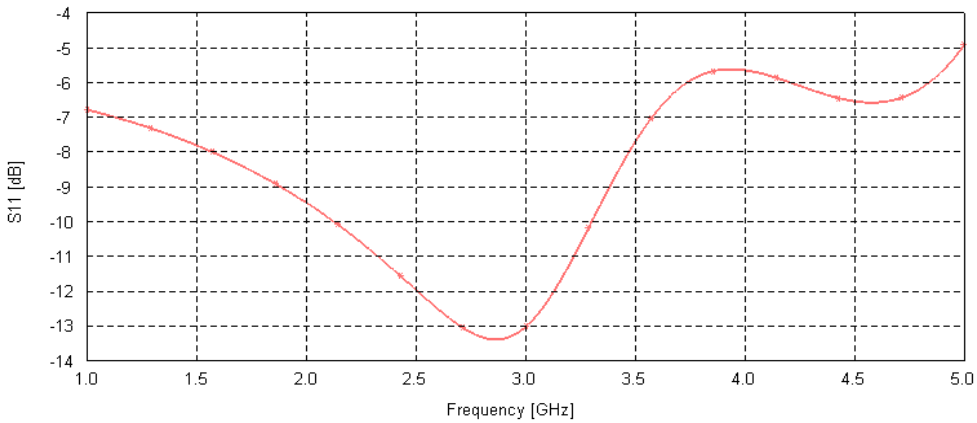

Figure 31: S11 results of the feed network simulated in FEKO.

The forward transmission behavior can be observed in Figure 32 and a zoomed in version is provided in Figure 33 for a more detailed analysis. The general behavior of the power levels are similar to the results obtained in ADS simulations. The level of power is about 11 dB below the input power in the band of interest. While the variation and trends stayed almost identical in simulations using both software packages, the average transmitted power level in FEKO is almost 3 dB lower than the level obtained in ADS. This decrease in the transmitted power was expected since FEKO, being an electromagnetic simulation tool, takes into account the radiation losses and other small effects that may cause power loss.

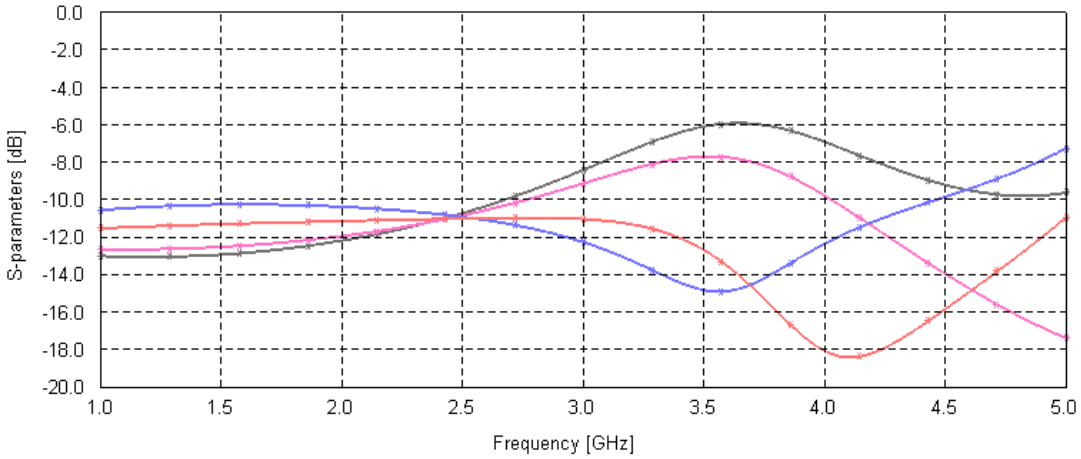

Figure 32: Transmission coefficient results of the feed network simulated in FEKO.

The difference between power levels to the output ports can be seen more clearly in Figure 33. The variation here is less than 0.5 dB in the band of interest as obtained in ADS. Looking at a wider range, it can be observed that the variation between the channels stays below 3 dB for a range of about 1 GHz.

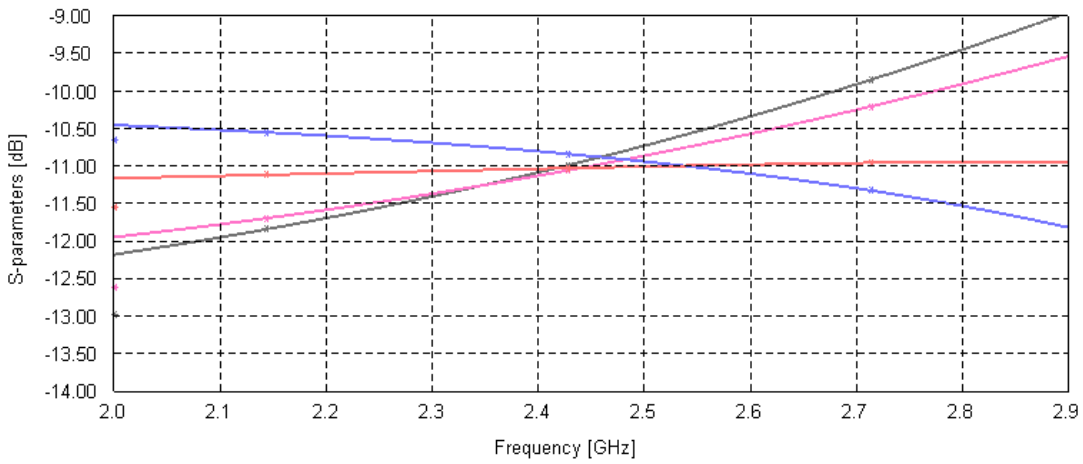

Figure 33: Transmission coefficient results of the feed network simulated in FEKO.

The phase difference between each of the output ports is shown in Figure 34. The difference between the closest port and the one next to it is 11 degrees. The next port has an additional delay of 13 degrees and the farthest port lags by another 4 degrees.

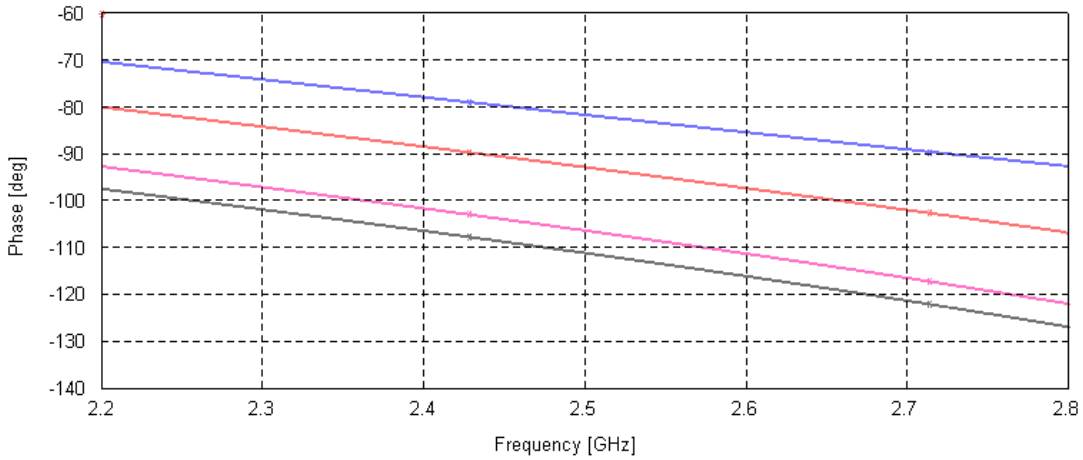

Figure 34: Phase of the output ports of the feed network simulated in FEKO.

3.4.3 Comparison with other Feed Structures

Two other comparable feed structures (the Butler Matrix and the Rotman Lens) were presented in section 2.4. The novel design presented in this thesis is better than these structures in two main aspects. The first aspect is the size; the size of the proposed feed network is significantly smaller than both of the compared structures. The

second aspect is two-dimensional steering capabilities; while the other feed networks can only drive linear arrays and steer the beam in one dimension, the proposed feed structure steers beams in two dimensions. It should be noted that the Butler Matrix and the Rotman Lens can be used to create arrays that can scan in two dimensions but more than one feed network is required for this.

3.5 Circular Array Design

This section describes the design process and presents the simulation results of the circular MSA array. The two main parts that were demonstrated in earlier sections, the circular feed network and the triangular MSA, were joined to create the circular array. The model was simulated and developed by making insightful modifications in FEKO since no theoretical model can be used for such a novel structure.

3.5.1 Earlier Work

Using a few active elements in this type of an array can result in beam steering as demonstrated by Fassetta and Sibille in [19]. In this work triangular MSAs were fed separately by coaxial probes where no phase shift was introduced. The circular array of triangular patches is also used by Sumantyo et al. in [20]-[22], where all the triangular elements were fed separately with coupled feeds.

3.5.2 Array Structure and Simulation Parameters

The array was formed by copying and rotating the triangular MSAs around the z-axis with 60-degree intervals and connecting them with the feed network designed in section 3.4. The resulting structure geometry is shown in Figure 35. In the later stages some modifications were made to the feed network geometry in order to improve the performance. However the triangular patches were not modified.

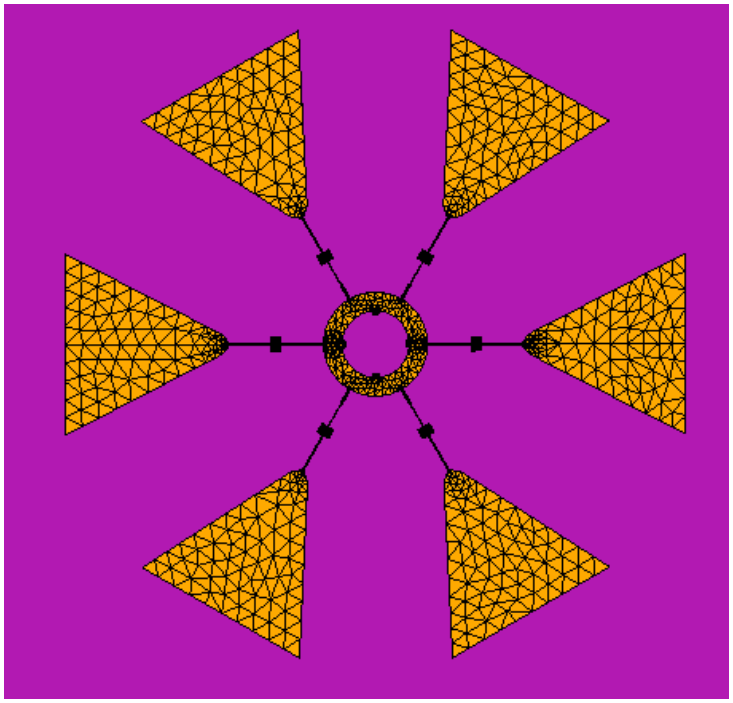

Figure 35: The circular array geometry composed of six equilateral triangular patches and the novel feed network.

The array is simulated with different input excitations in order to show the achieved steering in the beam direction. The first set data to be analyzed is the input reflection coefficient, since the antenna can't receive or transmit any power without proper matching. This data, which also gives the impedance bandwidth, should be analyzed for all active ports. All inactive ports are treated as open circuits. The ports are labeled as seen in Figure 36 to avoid ambiguity.

The transmission coefficients between the ports (S21, S31, etc.) are also important when the array is excited with more than one port. If the transmission coefficient is high between two input ports, too much power is delivered to the other active input port. This type of a system cannot possibly be efficient. In other words the isolation between the input ports should be high so that the power is transmitted to the triangular elements, not to the other input ports.

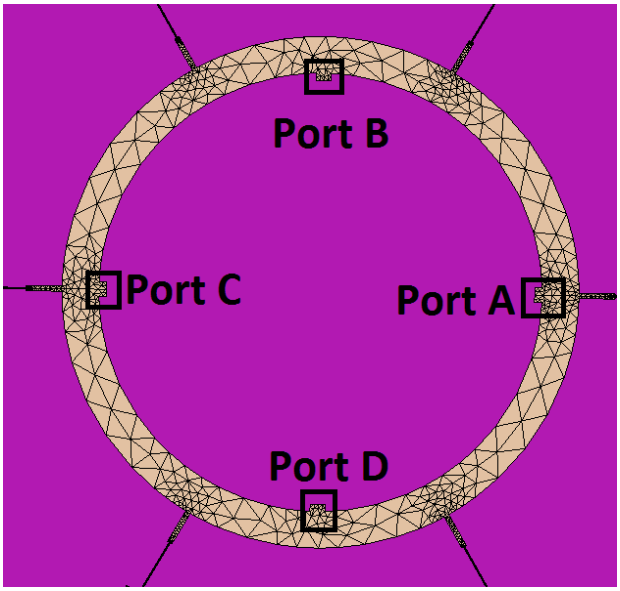

Figure 36: Distribution of ports on the circular feed network.

The radiation pattern is the important set of data that is used to characterize an antenna. This data primarily shows how much an antenna radiates in every direction but it also gives the gain and beamwidth of the antenna.

In the presented data, theta (θ) values give the amount of elevation down the z-axis which is perpendicular to the surface; so theta equals to zero degrees when the beam is perpendicular to the surface. Phi (Φ) values give the amount of rotation in the x-y plane, which is the surface that the antenna lays on. Therefore, phi equals to zero degrees in the direction where port A is located.

3.5.3 Unmodified Circular Array Simulation Results

The array presented in this section is composed of the previously designed circular feed network and six triangular MSAs. The dimensions of these parts were not modified in the creation of this array. Simulations with different excitation combinations are presented.

Simulation results with only port B excitation are presented as well only port A results, because the excitation of port A and B can't be regarded symmetrical. Port A is located at the same level with the feed point of a patch and port B is located between the feed points of two patches. Results obtained by the excitation of port C or D are not presented since they are completely symmetrical with the mentioned cases. A similar approach is used for multiple port combinations, also without presenting the symmetrical cases.

Port A: Figure 37 shows the input reflection coefficient at port A, which indicates that the array has acceptable insertion loss between 2.3 and 2.7 GHz.

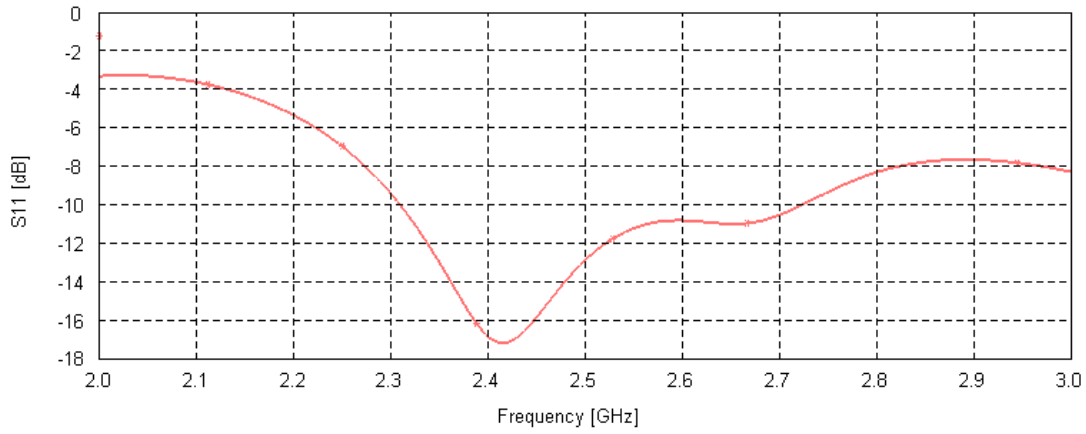

Figure 37: Input reflection coefficient at port A, when it's the only excited port.

The max gain is 7.6 dB at the main lobe, which is tilted towards the direction of port A as seen in Figure 38. The angle of steering and the beamwidth can be read more clearly in the two-dimensional radiation pattern given in Figure 39. The amount of steering is 13 degrees from the z-axis and the beamwidth is 25 degrees in the elevation plane.

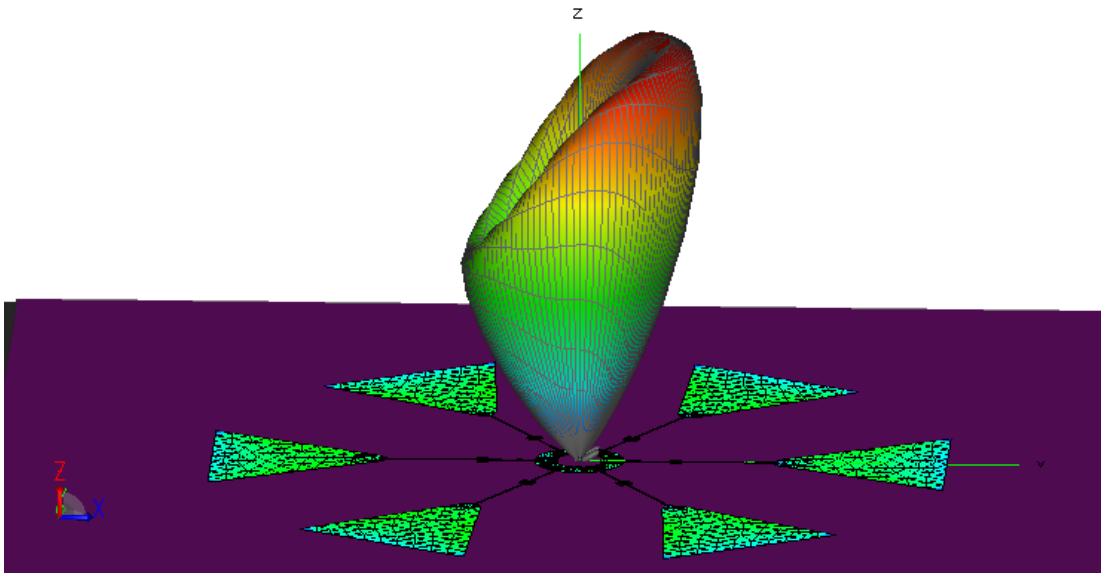

Figure 38: 3-D radiation pattern in linear scale, when only port A is excited.

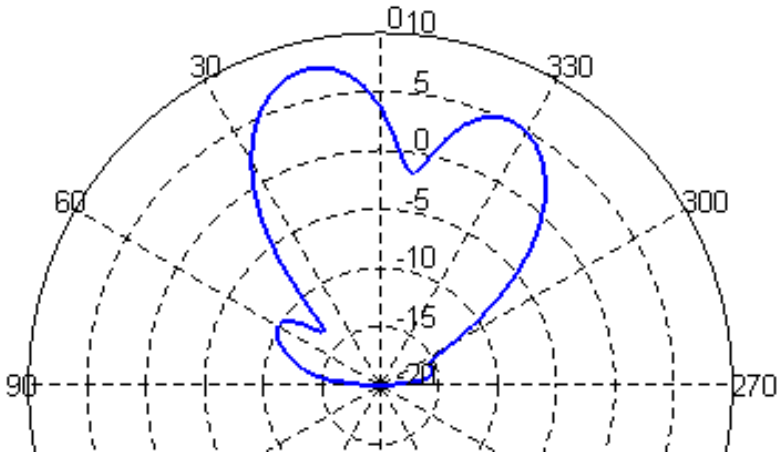

Figure 39: Radiation pattern in decibel scale in $\Phi=0^{o}$ plane, when only port A is excited.

Port B: Although port B is located between two junctions, unlike port A, all of the results for this configuration are almost identical to the port A results. The only difference is in the direction of radiation, which is this time, steered in the direction of port B. In other words the main lobe rotated 90 degrees anti-clockwise in the phi

plane. This result was highly desired and anticipated, since it confirms that this novel structure can radiate in different directions depending on the port selection.

Ports A and B: This is the first example where more than one port is excited. Analysis becomes more complex when there is more than one port involved. In this case the most important parameter that needs to be added to the analysis is the transmission coefficient. This parameter gives the influence of ports on each other. In earlier simulations, in section 3.4, transmission needed to be maximized between the input port and the output ports. However, in this case, transmission coefficient needs to be kept at a minimum between the input ports, so that the power is not lost. In other words, a high isolation is desired between the input ports.

The input matching obtained with this configuration is not as good as the performance obtained when a single port is excited, however, it is within acceptable limits. The impedance bandwidth is found to be around 350 MHz, between 2.41 and 2.76 GHz for both ports as seen in Figure 40.

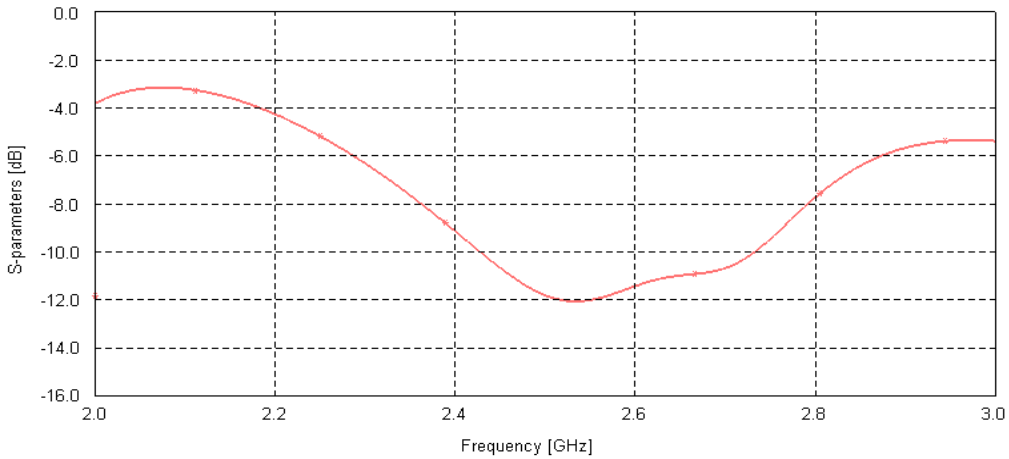

Figure 40: Input reflection coefficient at port A and port B.

The next graph, given in Figure 41, shows the transmission between port A and port B. The result here is less than satisfying; about 40 percent of the power is lost around 2.4 GHz. This indicates that modifications should be made to increase the amount of isolation between the input ports.

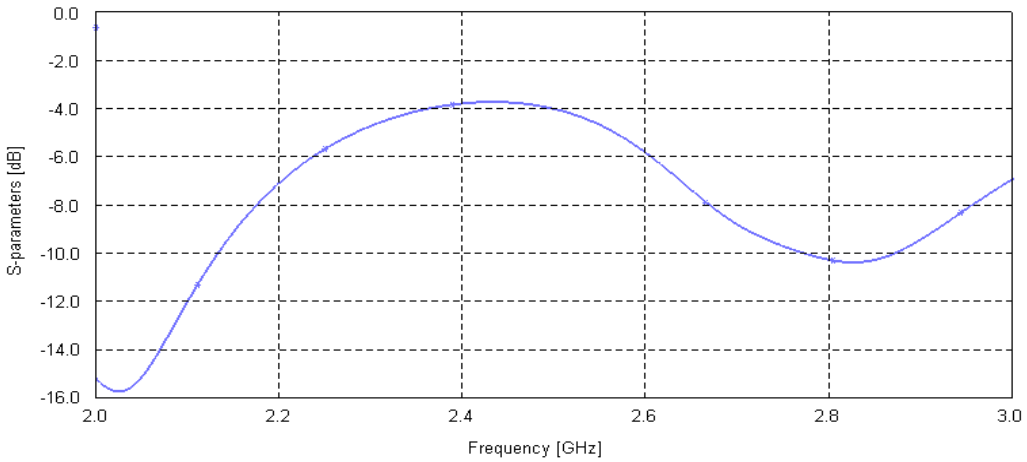

Figure 41: Transmission coefficient (S21) between port A and B.

Although some parameters need to be improved the array does what it is designed for. Again the steering is achieved in the intended manner between ports A and B, which is seen in Figure 42. The main beam is rotated 45 degrees in the anti-clockwise direction from the point where port A is located.

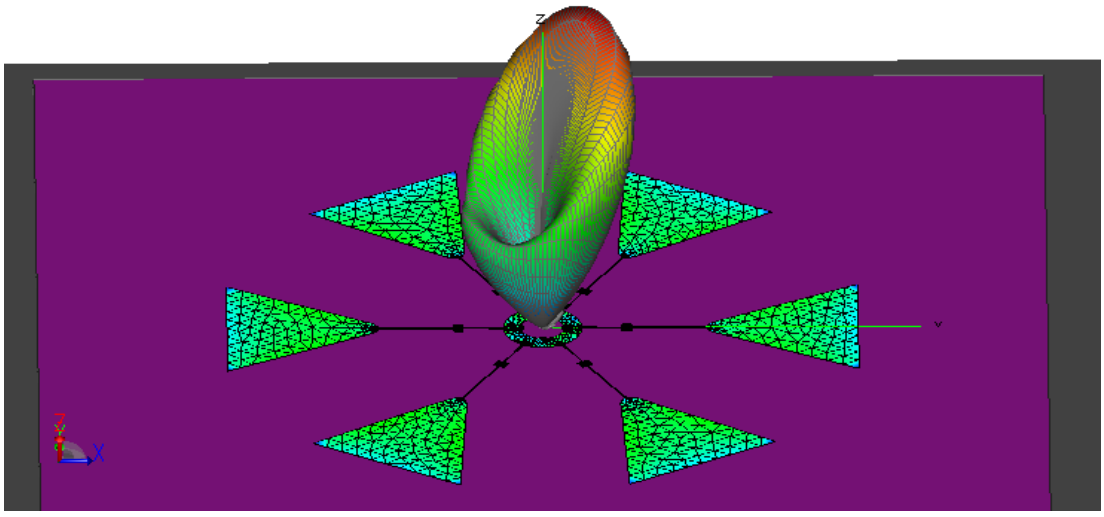

Figure 42: 3-D radiation pattern in linear scale, when port A and B are excited.

The main beam is 12 degrees from the z-axis with a beamwidth of 25 degrees and the gain reaches 5.5 dB. These values can be seen more clearly in Figure 43, which cuts the main beam at phi equals 45 degrees.

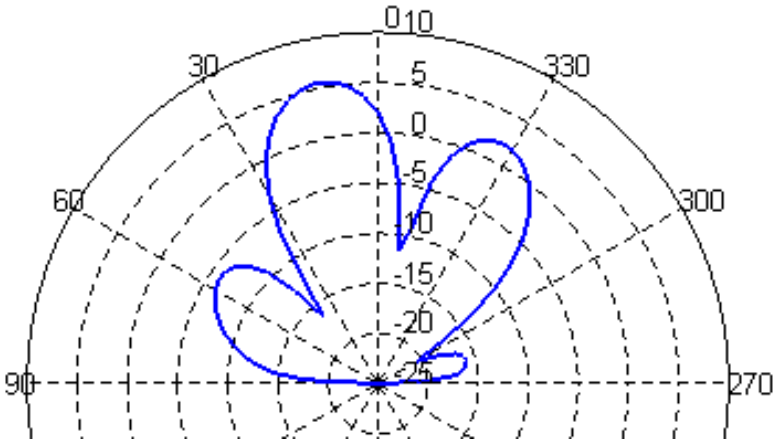

Figure 43: Radiation pattern in decibel scale in $\Phi=45^{o}$ plane, when ports A and B are excited.

Ports A, B and C: This configuration results in a similar radiation pattern to the one obtained when only port B is excited (Figure 44). Although a higher gain was anticipated from this configuration, results show that the gain is lower in this case.

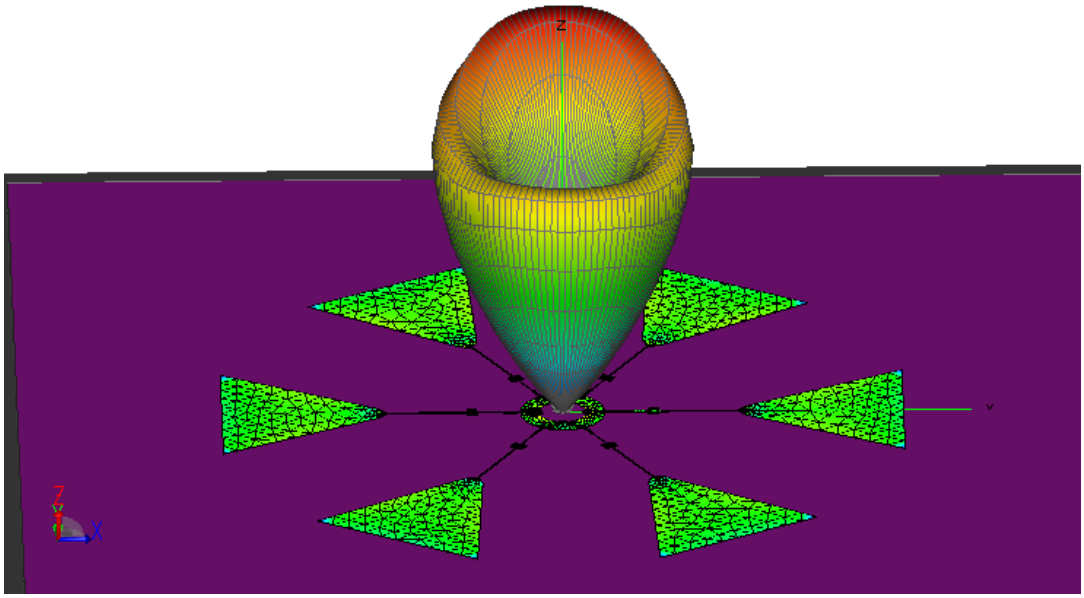

Figure 44: 3-D radiation pattern in linear scale, when port A, B and C are excited.

Figure 45 shows that the main beam is 15 degrees down from the z-axis and the beamwidth is about 22 degrees with a maximum gain that reaches 5 dB. The side lobe is relatively bigger in this configuration compared to the others.

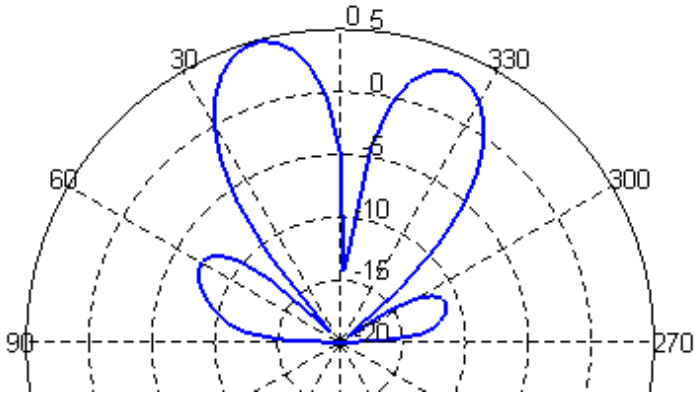

Figure 45: Radiation pattern in decibel scale in $\Phi=90^{o}$ plane, when ports A, B and C are excited.

The reflection coefficient for ports A and C are identical as they are symmetrical. The reflection coefficient for these ports is presented in Figure 46. Here, a mismatch is observed, due to a shift towards the higher frequencies. This shows the importance of having a wideband system, especially in systems like this, where different combinations result in different characteristics. This problem should be solved by modifying the feed structure.

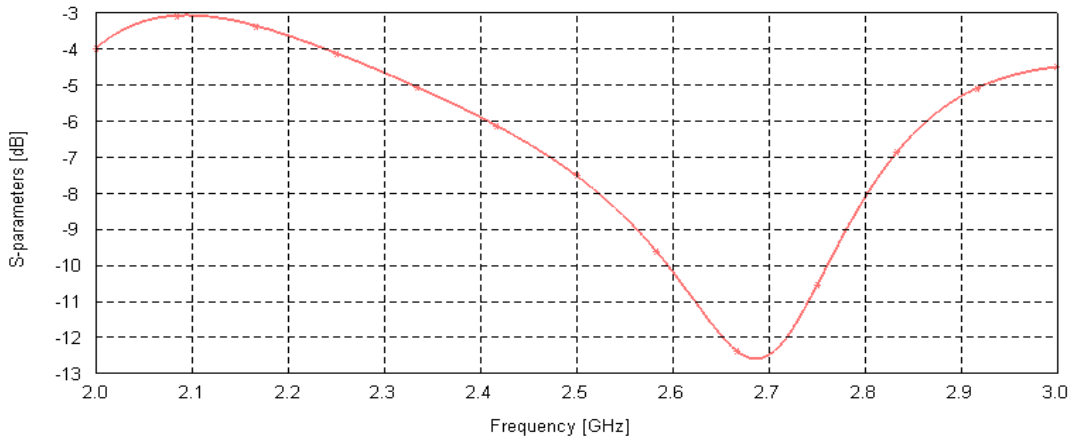

Figure 46: Input reflection coefficient at ports A and C, when ports A, B and C are excited.

The matching condition for port B is also poor as it can be observed in Figure 47, where the input reflection coefficient is never below -10 dB.

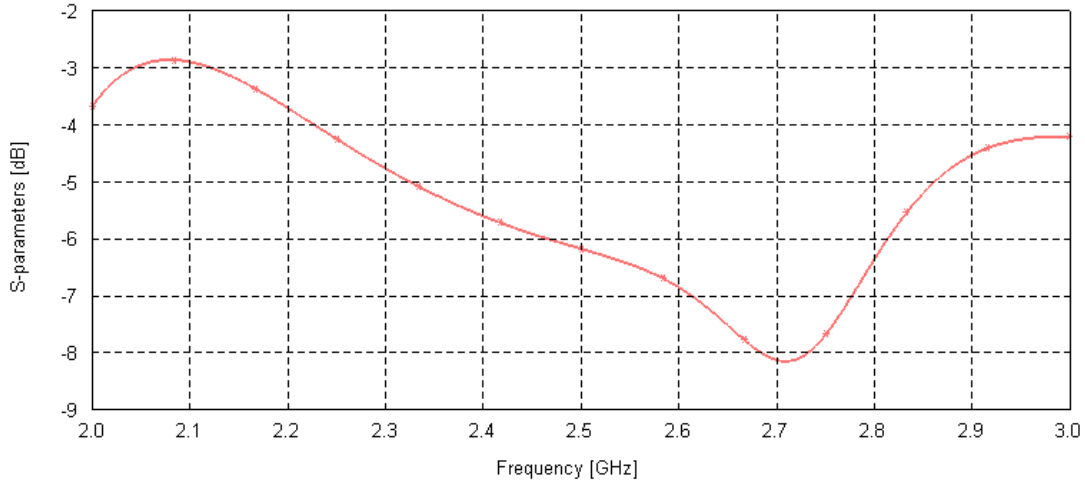

Figure 47: Input reflection coefficient at port B, when ports A, B and C are excited.

The transmission coefficients are illustrated in Figure 48. The upper line shows the relationship between ports A and C. The lower line shows the isolation relationship between ports A and B. The relationship between ports C and B coincides with the lower line due to the symmetry. The isolation between the ports is not as high as desired. Too much power is transmitted to other input ports, causing losses.

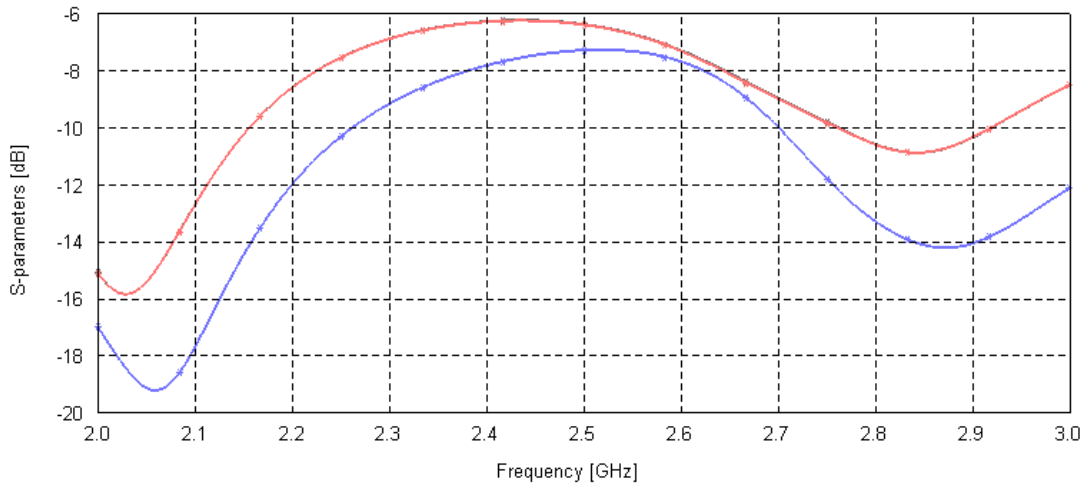

Figure 48: Transmission coefficients between ports A, B and C.

Ports A and C: This configuration gives rise to two main beams which will allow communication in two directions at the same time. The input matching characteristics seem to be good except that the range is shifted towards the higher frequencies. Similar trend were also observed in previous configurations which mean that this problem can be fixed for all the configurations at the same time with modifications to the feed network. The reflection coefficients at both ports are equal due to the symmetry and given in Figure 49.

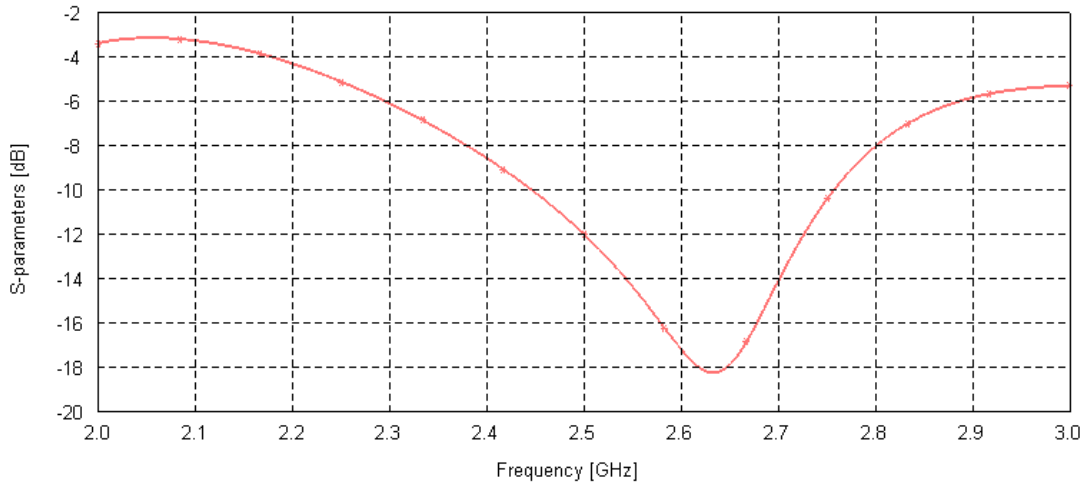

Figure 49: Input reflection coefficient at port A and port C, when ports A and C are excited.

The dual-beam radiation can be observed in Figure 50 where main beams are located at about 22 degrees from the z-axis. The beams are found at phi equals 90 and -90 degrees. The problem in this pattern is the high amount of radiation in other directions. The performance should be improved to diminish the radiation at the sides.

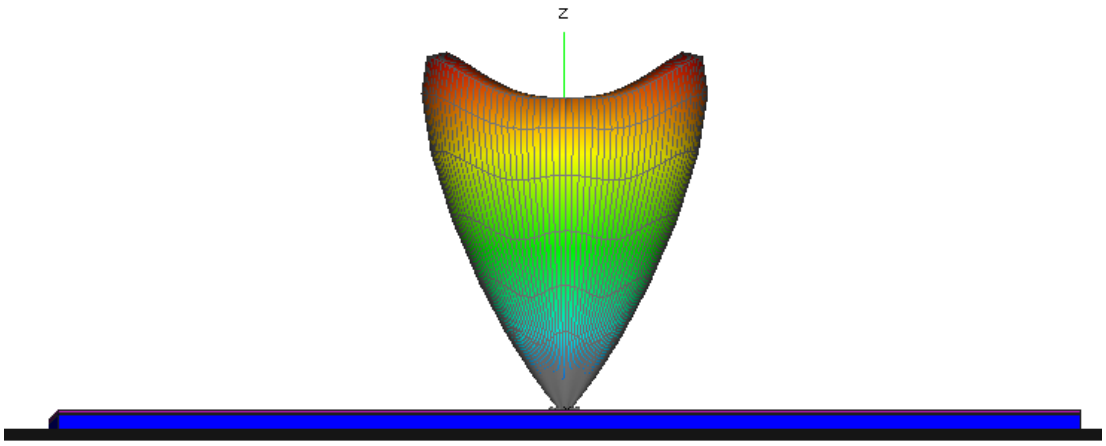

Figure 50: 3-D radiation pattern in linear scale, when ports A and C are excited.

Beamwidth of both beams is 25 degrees. However, the gain does not exceed 5 dB. This is mostly due to the division of power between the two lobes.

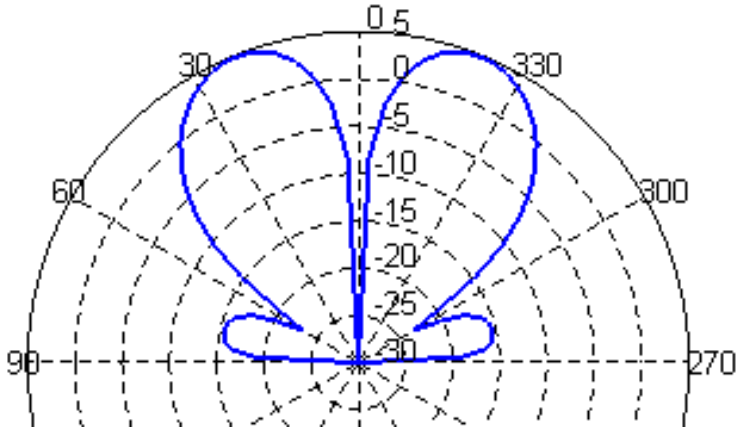

Figure 51: Radiation pattern in decibel scale in $\Phi=90^{o}$ plane, when ports A and C are excited.

The isolation between the input ports is also too low in this configuration. This is illustrated in Figure 52 where transmission coefficient between the ports becomes as high as -4 dB in the range of interest.

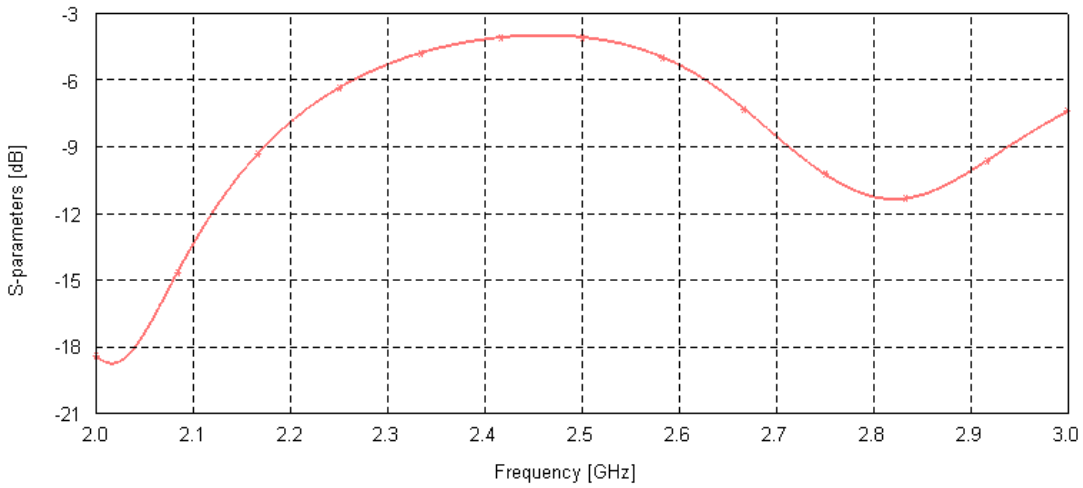

Figure 52: Transmission coefficient between ports A and C.

Summary: Although the presented initial design proves the concept of beam steering using the novel feed network, it needs to be improved before it can be practical. Some of the problems to be addressed in order to improve the performance of the array are as follows:

1. High side lobes.
2. Poor isolation between the input ports.
3. Too wide beamwidth in the azimuth plane.
4. Low gain.
5. Shift of the matching frequency.
6. Limited steering angle.

3.5.4 Improved Circular Array: Simulation Results

The final version of the array is presented in this section with the applied modifications. One of the first modifications was to increase the diameter of the ring to improve the isolation between the input ports. This also helped to solve the problem of shifted matching frequency. Then the lengths of the feed lines that connect the patches to the ring were increased to obtain a better matching.

Port A: The input reflection coefficient when only port A is excited can be seen in Figure 53. The reflection coefficient is less than -9 dB from 2.06 to 2.8 GHz for a total range of 740 MHz, which is about 340 MHz wider than the previous result as shown in Figure 37. The reflection coefficient is below -11 dB in the range of interest.

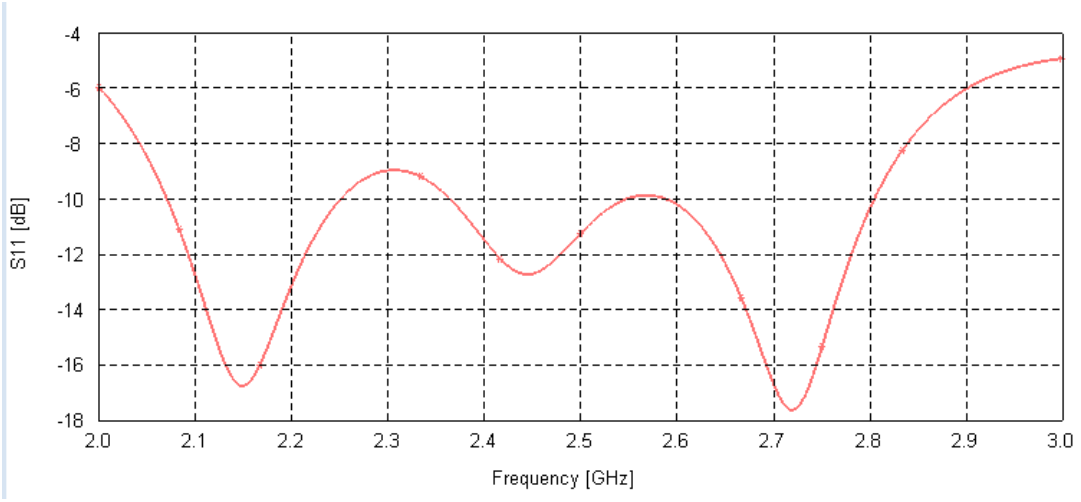

Figure 53: Input reflection coefficient at port A, when it's the only excited port (after improvements).

The final antenna has a gain of 8.3 dB at the peak of the steered beam when excited through a single port and the main beam is about 10 degrees off the z-axis as seen in Figure 54. The beamwidth of the main beam is around 20 degrees. These results indicate an improvement of 0.7 dB in the gain. Additionally, the side lobe levels are also lower and the beamwidth in the azimuth plane has become more focused. However, the steering angle was diminished by 5 degrees.

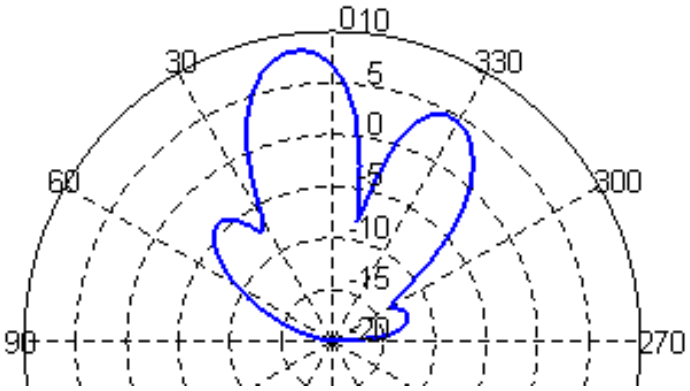

Figure 54: Radiation pattern in decibel scale for phi = 0^{o}, when port A is excited (after improvements).

The three-dimensional radiation pattern is given in Figure 55 with a linear scale showing the amount of steering.

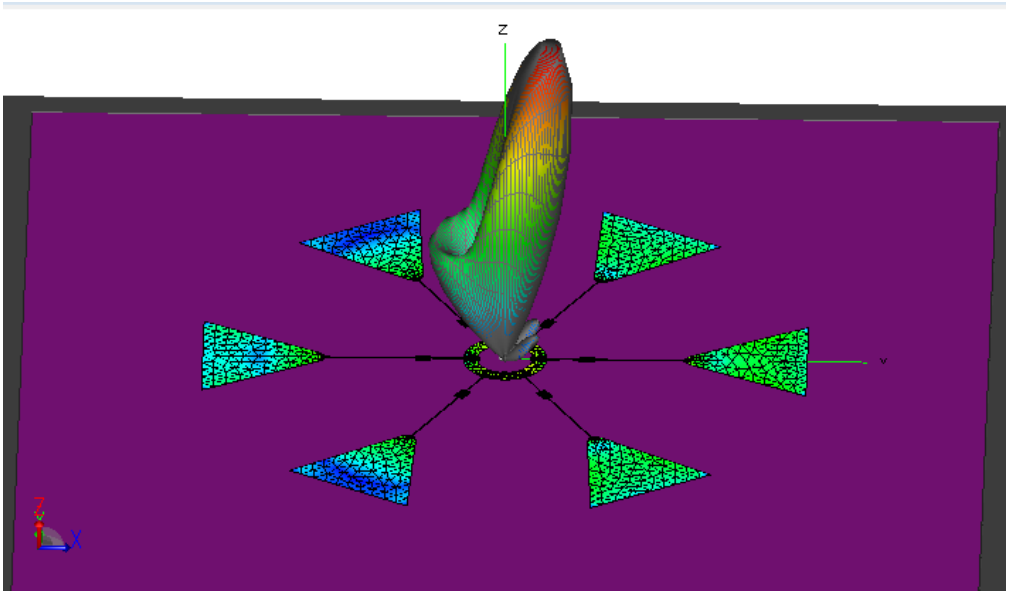

Figure 55: 3-D radiation pattern in linear scale, when port A is excited (after improvements).

Port B: All results obtained for port B excitation are similar to port A results except for the rotation in direction. Gain, beamwidth and matching conditions were found to be almost identical to the values obtained with port A excitation.

Ports A and B: Excitation of two consecutive ports gives rise to a beam between these ports as shown in the previous section. The input reflection coefficient and the isolation between the ports were not as good as desired in the previous design. The modifications made here improved these parameters. The input reflection coefficient can be seen in Figure 56 and the transmission coefficient is given in Figure 57.

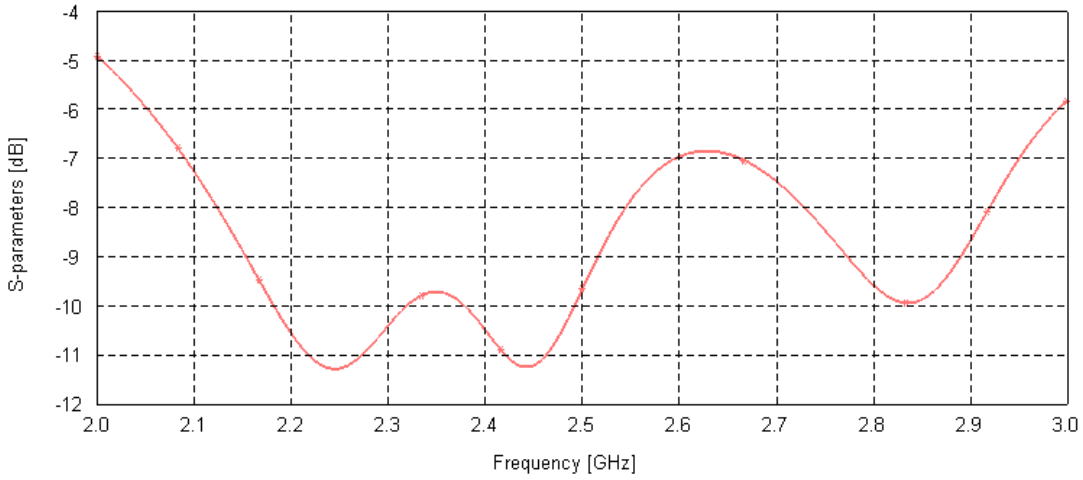

Figure 56: Input reflection coefficient at port A, when it's the only excited port (after improvements).

The matching conditions were not improved much. However, the isolation between the ports was greatly improved; the transmission coefficient is below –11 dB within the band of interest. This was achieved by modifying the feed structure to shift the resonant frequency so that there is a high isolation in the band of interest.

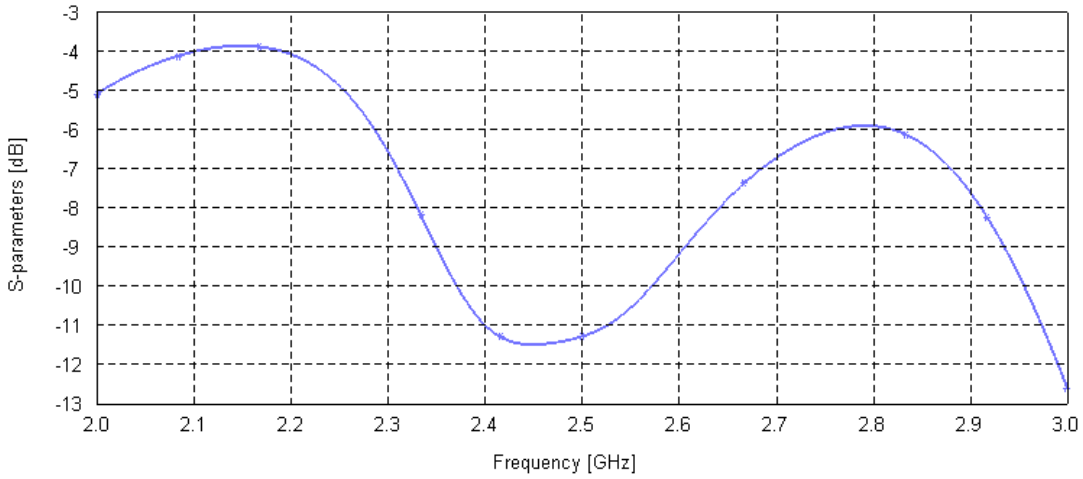

Figure 57: Transmission coefficient (S21) between ports A and B (after improvements).

The radiation pattern of this configuration is given in Figure 58 at the cut plane of phi equals 45 degrees and in Figure 59 as a three-dimensional snapshot. Figure 58 shows that the main beam has a gain of 6 dB at the peak which is slightly higher than the previous result. The main beam is 10 degrees down the z-axis and the beamwidth is 20 degrees.

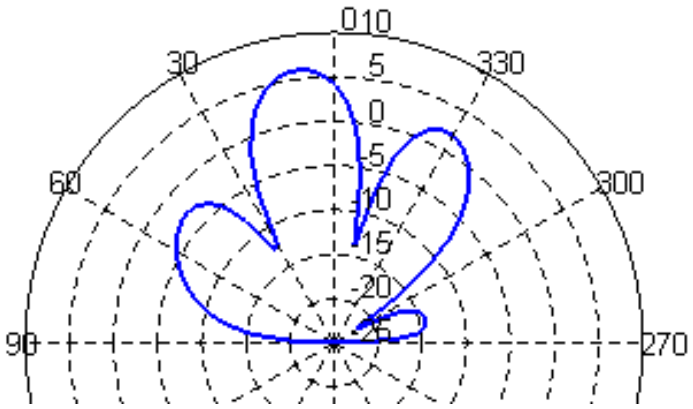

Figure 58: Radiation pattern in decibel scale for phi = 45^{o}, when ports A and B are excited (after improvements).

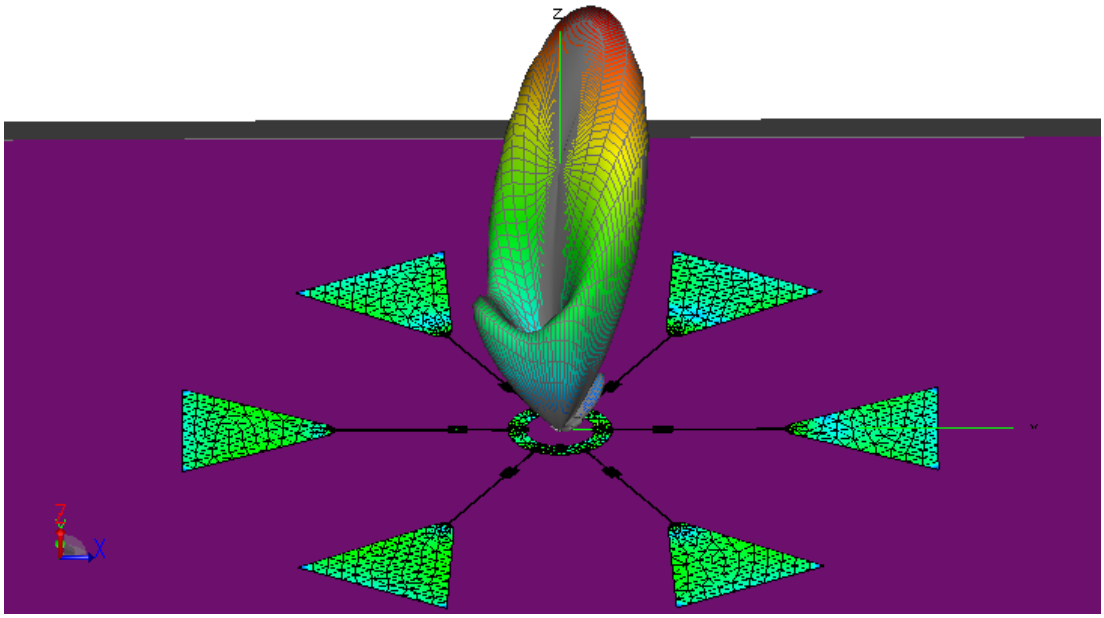

Figure 59: 3-D radiation pattern in linear scale, when ports A and B are excited (after improvements).

Ports A, B and C: This type of a configuration gives a beam in the same direction as when the middle port is excited. In this case the main beam is in the direction of port B. The input reflection coefficient shown in Figure 60 indicates an impedance bandwidth of 170 MHz from 2.34 to 2.51 GHz at ports A and C. The input reflection coefficient for port B is given in Figure 61 where matching is not as good as desired but again there is improvement when compared to the previous result in Figure 47.

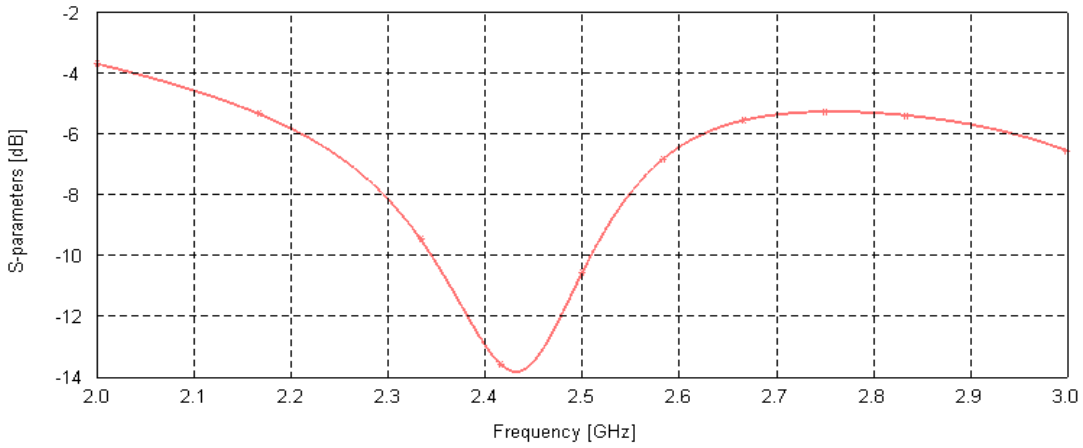

Figure 60: Input reflection coefficient at port A and C, when ports A, B and C are excited (after improvements).

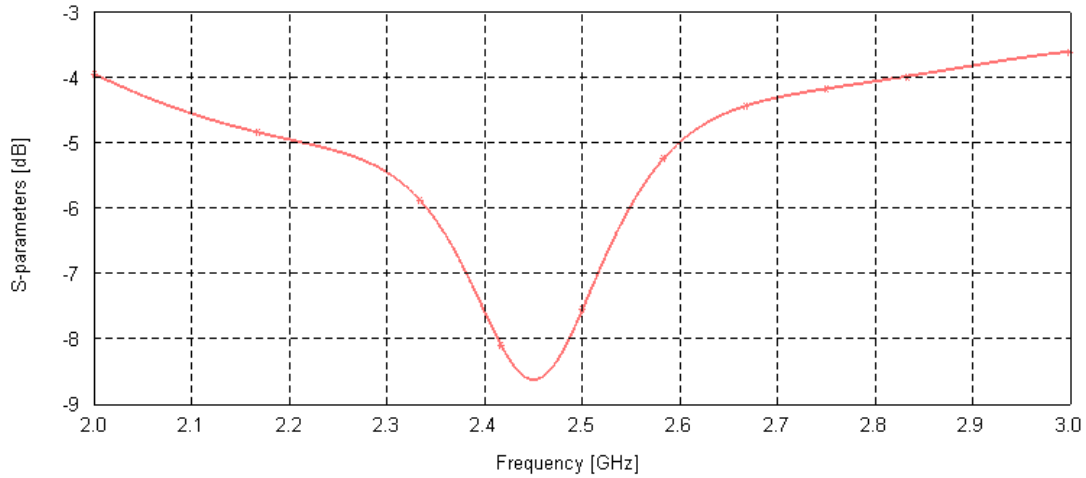

Figure 61: Input reflection coefficient at port B, when ports A, B and C are excited (after improvements).

The isolation between the ports is given in Figure 62. The line that dips lower gives the relationship between ports A and C. The other line gives the relationship between ports A and B and also between C and B due to the symmetry.

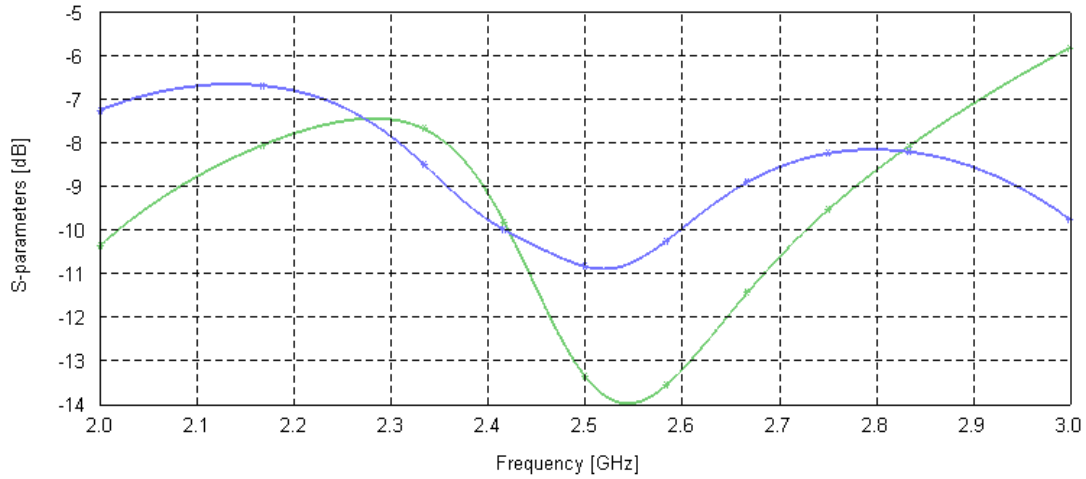

Figure 62: Isolation between the ports when ports A, B and C are excited (after improvements).

Although this three-port configuration gave high gain values in some of the tested setups, better isolation and higher gains at single port configurations were favored in

the final configuration. Therefore, this configuration was in a way sacrificed, since a beam in the same direction can also be obtained by the excitation of a single port.

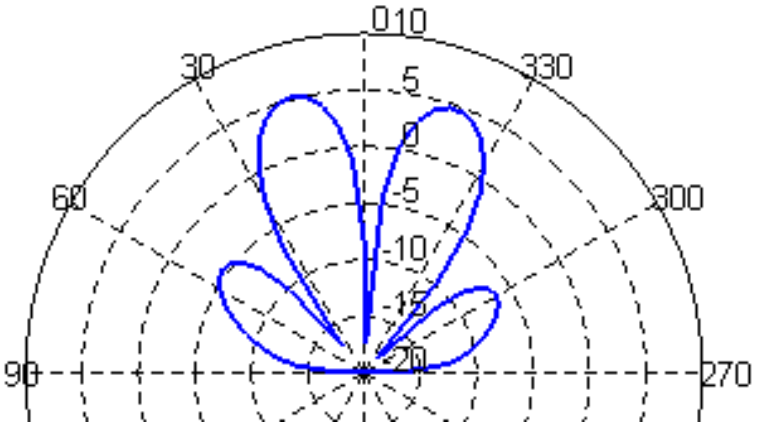

Figure 63: Radiation pattern in decibel scale for phi = 90^{o}, when ports A, B and C are excited (after improvements).

The three-dimensional radiation pattern, given in Figure 64, doesn't show much improvement. The maximum gain is still around 5 dB.

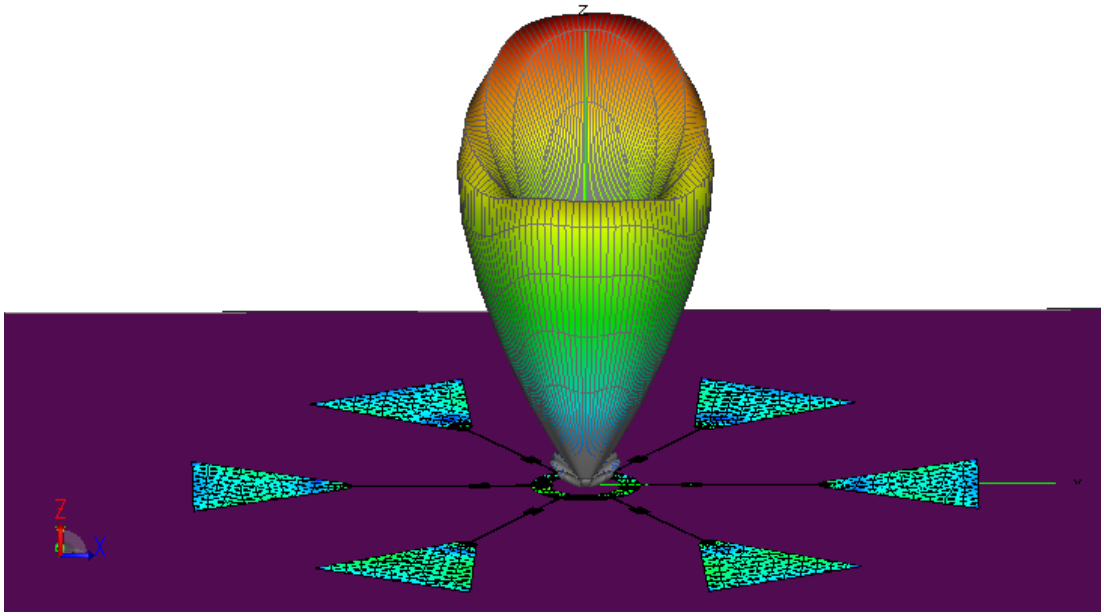

Figure 64: 3-D radiation pattern in linear scale, when ports A, B and C are excited (after improvements).

Ports A and C: The dual-beam operation, which was obtained with ports A and C, was also improved by the modifications. The input reflection coefficient shown in Figure 65 was identical for both ports due to symmetry. The impedance bandwidth is about 290 MHz and it is shifted by 200 MHz towards the band of interest compared to the previous result shown in Figure 49. The band now spans 2.26 to 2.55 GHz.

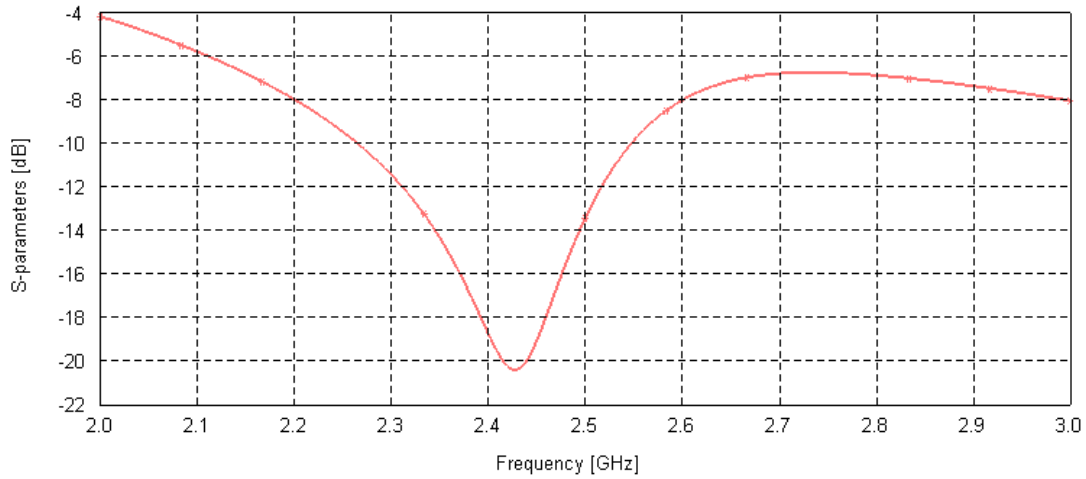

Figure 65: Input reflection coefficient at port A and port C, when ports A and C are excited (after improvements).

The isolation between the ports was improved and it is given in Figure 66. This is a significant improvement when compared to the results in Figure 52.

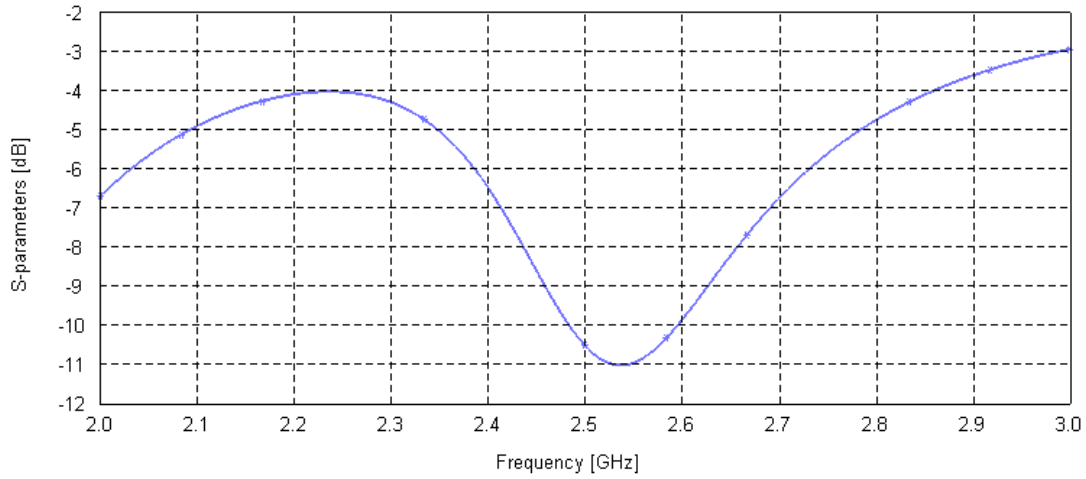

Figure 66: Transmission coefficient (S21) between ports A and C (after improvements).

A gain of 5 dB was obtained at the peak which can be observed in Figure 67. The beams are steered 20 degrees off the z-axis and have a beamwidth of 20 degrees. The main lobes became more concentrated in the azimuth plane, which can be observed in the three-dimensional radiation pattern in Figure 68.

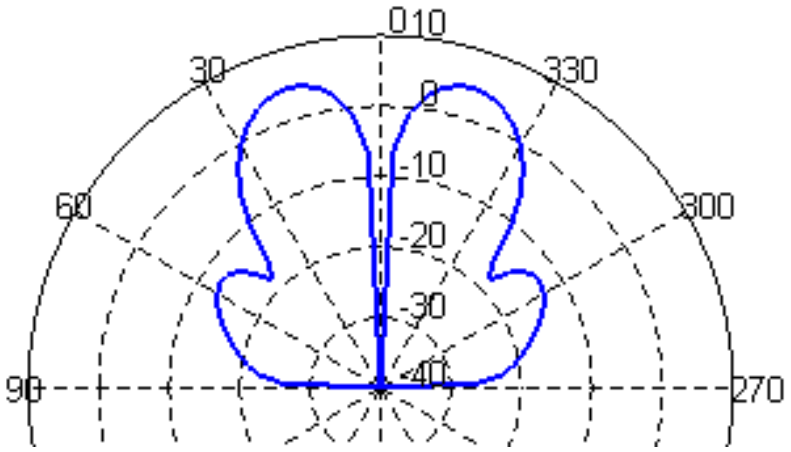

Figure 67: Radiation pattern in decibel scale for phi = 0^{o}, when ports A and C are excited.

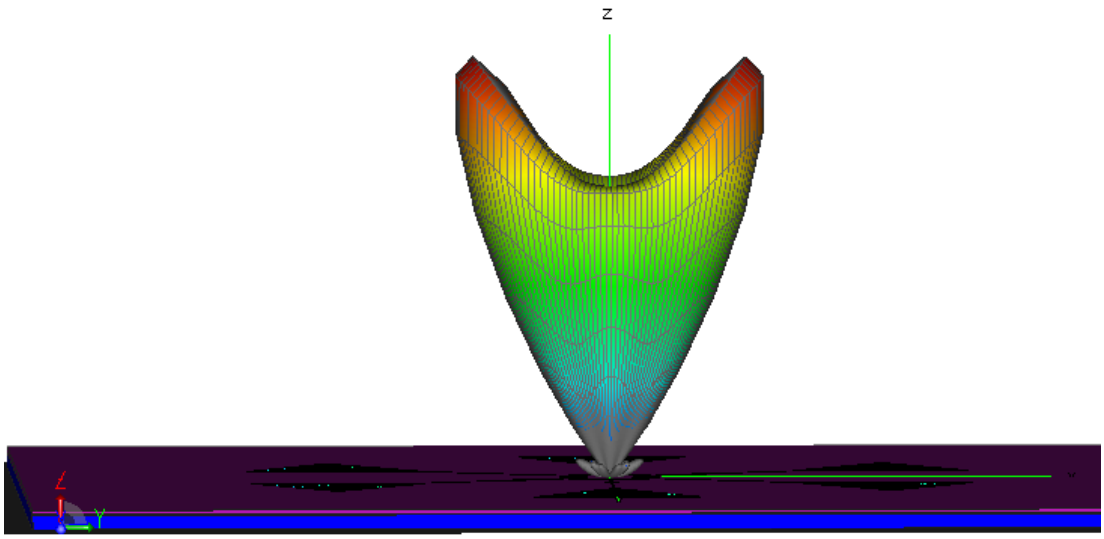

Figure 68: 3-D radiation pattern in linear scale, when ports A, B and C are excited (after improvements).

Summary: The performance of the antenna was improved with the final modifications, especially addressing the isolation problems and shifts at the matching frequency. High side lobes were diminished in some cases and more focused beams were obtained. However, in some cases sacrifices had to be made since the levels of isolation between the ports weren't acceptable. For example the limited steering angle issue still needs to be worked on.

The final dimensions of the modified circular array are given in Figure 69. Note that no changes were made to the size of the patch elements.

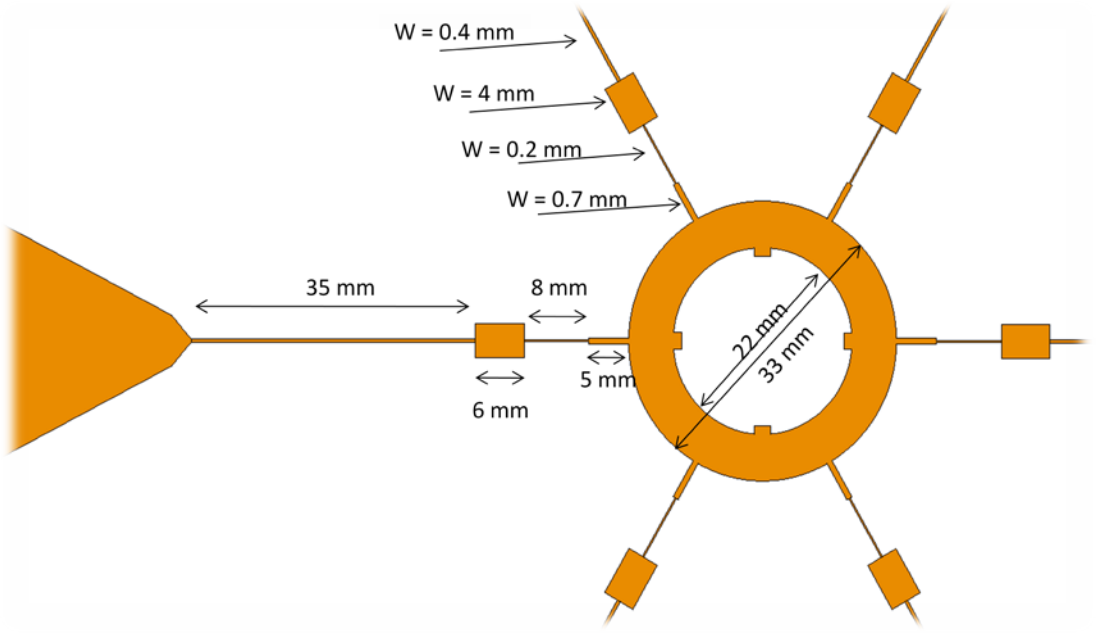

Figure 69: The final feed network dimensions.

Similar patterns and gain were obtained at different directions when different port combinations were used. A summary of steering angles and directions obtained through different feed combinations can be seen in Table 3. It should be noted that

combinations that are symmetrical with one of the presented cases are not shown in the table.

Table 3: Change of radiation direction obtained through excitation of different port combinations.

Excited Ports	**Main Beam Properties**	**Graphical Representation of Steering Direction**
A	$\Phi = 0^o$ $\Theta = 10^o$ Gain = 8.3 dB Beamwidth = 20 ^{o}	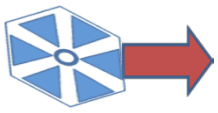
A and B	$\Phi = 45^o$ $\Theta = 10^o$ Gain = 6 dB Beamwidth = 20 ^{o}	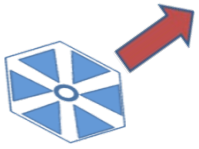
B	$\Phi = 90^o$ $\Theta = 10^o$ Gain = 8.3 dB Beamwidth = 20 ^{o}	
A and C (Dual- Beam)	$\Phi_1 = 0^o$ $\Phi_2 = 180^o$ $\Theta = 20^o$ Gain = 5 dB Beamwidth = 20 ^{o}	
A,B and C	$\Phi = 90^o$ $\Theta = 10^o$ Gain = 5 dB Beamwidth = 20 ^{o}	

Chapter 4

CONCLUSION and RECOMMENDATIONS

4.1 Conclusion

A novel two-dimensional passive beam steering antenna array has been presented in this thesis [27]. The array utilizes a novel 6-way circular power divider as the feed network and equilateral triangular patch antennas as the array elements. Steering of the beam direction has been achieved through the phase delay introduced by the off-center feed structure of the novel circular feed network. Beam direction selection by exciting different ports has been successfully applied and shown in the simulation results. The proposed array is significantly smaller and easier to build than the existing multi-directional arrays.

4.2 Recommendations and Future Work

The feed network can be improved by placing a ground in close proximity to limit the amount of loss through radiation. The most practical way of implementing this would be placing a ground plane underneath the FR-4 substrate right below the feed structure. This ground plane should only be present below the feed lines. An alternative solution could be implemented by using a co-planar structure to place ground lines near the feed lines to limit radiation. In either of these cases, the feed network would have to be redesigned to account for the changes in the characteristic impedances of the feed lines.

REFERENCES

[1] Deschamps, G. A. "Microstrip Microwave Antennas." *3rd USAF Symposium on Antennas*, 1953.

[2] Munson, R.; , "Conformal microstrip antennas and microstrip phased arrays," *Antennas and Propagation, IEEE Transactions on* , vol.22, no.1, pp. 74- 78, Jan 1974.

[3] Balanis, Constantine A. "Chapter 14: Microstrip Antennas." *In Antenna Theory: Analysis and Design, 2nd Edition*. New York, NY: Wiley, 1996.

[4] James, J. R.. *Handbook of Microstrip Antennas (IEE Electromagnetic Waves Series, 28) (2-Vol Box Set)* London: The Institution of Engineering and Technology, 1988.

[5] Milligan, Thomas *A.*. *Modern Antenna Design. 2 ed*. New York: Wiley-IEEE Press, 2005.

[6] Navy, Naval Air Systems Command United States. *Electronic Warfare and Radar Systems Engineering Handbook.* Washington, D.C. : Naval Air Systems Command, 1992.

[7] HARISANKAR, N.S. "More About Antennas." *Ham Radio And Electronics Website* : Ham Radio India. http://hamradio.in/circuits/more_on_antennas.php (accessed May 29, 2010).

[8] Butler J.; Lowe R.; , “Beam forming matrix simplifies design of electronically scanned antennas,” *Electronic Design*, vol.9, pp. 170–173, Apr. 1961.

[9] Rotman, Walter. 1965 “Multiple beam radar antenna system” U.S. Patent 3,170,158, filed May 8 1963, and issued February 16, 1965.

[10] Rotman, W.; Turner, R.; , "Wide-angle microwave lens for line source applications," *Antennas and Propagation, IEEE Transactions on* , vol.11, no.6, pp. 623- 632, Nov 1963.

[11] Dahele, J.; Kai Lee; , "On the resonant frequencies of the triangular patch antenna," *Antennas and Propagation, IEEE Transactions on* , vol.35, no.1, pp. 100- 101, Jan 1987.

[12] Guha, D.; Siddiqui, J.Y.; , "Resonant frequency of equilateral triangular microstrip antenna with and without air gap," *Antennas and Propagation, IEEE Transactions on* , vol.52, no.8, pp. 2174- 2178, Aug. 2004.

[13] Guha, D.; , "Resonant frequency of circular microstrip antennas with and without air gaps," *Antennas and Propagation, IEEE Transactions on* , vol.49, no.1, pp.55-59, Jan 2001.

[14] Pham, N.T.; Gye-An Lee; De Flaviis, F.; , "Microstrip antenna array with beamforming network for WLAN applications," *Antennas and Propagation Society International Symposium, 2005 IEEE* , vol.3A, no., pp. 267- 270 vol. 3A, 3-8 July 2005.

[15] Kim, J.; Cho, C.S.; Barnes, F.S.; , "Dielectric Slab Rotman Lens for Microwave/Millimeter-Wave Applications," *Microwave Theory and Techniques, IEEE Transactions on* , vol.53, no.8, pp. 2622- 2627, Aug. 2005.

[16] Agilent Technologies, “Advanced Design System (ADS) ver. 2006A”, Santa Clara CA 95051, United States, http://www.home.agilent.com.

[17] EM Software & Systems - S.A. (Pty) Ltd, Stellenbosch, South Africa: FEKO - Field Computations Involving Bodies of Arbitrary Shape, Suite ver. 5.5, http://www.feko.info.

[18] EM Software & Systems - S.A. (Pty) Ltd, Stellenbosch, South Africa: “FEKO User’s Manual Suite ver. 5.5” July 2009, http://www.feko.info.

[19] Fassetta, S.; Sibille, A.; , "Low-profile circular array of equilateral triangular patches for angular diversity," *Microwaves, Antennas and Propagation, IEE Proceedings* - , vol.150, no.1, pp. 34- 36, Feb. 2003.

[20] Sumantyo, J.T.S.; Ito, K.; Takahashi, M.; , "Dual-band circularly polarized equilateral triangular-patch array antenna for mobile satellite communications,"

Antennas and Propagation, IEEE Transactions on , vol.53, no.11, pp. 3477-3485, Nov. 2005.

[21] Sumantyo, J.T.S.; Ito, K.; , "Circularly polarised equilateral triangular patch antenna for mobile satellite communications," *Microwaves, Antennas and Propagation, IEE Proceedings* - , vol.153, no.3, pp. 282- 286, June 2006.

[22] Tanaka, T.; Sumantyo, J.T.S.; Kaneko, K.; Ishide, D.; Takahashi, M.; Ito, K.; Yamamoto, S.; Miura, A.; , "Mobile communications experiments on dual-band triangular-patch array antenna using a pseudo satellite," *Antennas and Propagation Society International Symposium, 2005 IEEE* , vol.3B, no., pp. 277- 280 vol. 3B, 3-8 July 2005.

[23] Ibrahim, S.Z.; Rahim, M.K.A.; Masri, T.; Karim, M.N.A.; Abdul Aziz, M.Z.A.; , "Multibeam Antenna Array with Butler Matrix for WLAN Applications," *Antennas and Propagation, 2007. EuCAP 2007. The Second European Conference on* , vol., no., pp.1-5, 11-16 Nov. 2007.

[24] Hui Li; Feng, Z.H.; , "Switched planar hexagonal array of equilateral triangle patches for HIPERLAN terminals," *Microwave and Millimeter Wave Technology, 2004. ICMMT 4th International Conference on, Proceedings* , vol., no., pp. 204- 206, 18-21 Aug. 2004.

[25] CIA. "The World Factbook." *Central Intelligence Agency*. https://www.cia.gov/library/publications/the-worldfactbook/rankorder/2151rank. html (accessed April 24, 2010).

[26] Chen, Zhi Ning, and Michael Yan Wah Chia. *Broadband Planar Antennas: Design and Applications*. New York, NY: Wiley, 2006.

[27] Konca, M.; Uysal, S.; , "Circular Multi-Directional Patch Antenna Array with Selectable Beams Using a Novel Feed Structure and Equilateral Triangular Patches," *Mediterranean Microwave Symposium, Middle East Technical Univ. Northern Cyprus Campus, August 2010,* (Submitted for publication)

[28] "NEMA." *National Electrical Manufacturers Association*. N.p., n.d.. <http://www.nema.org/>, (accessed 30 May 2010)

APPENDIX

FR-4 Substrate Properties

FR-4 stands for “flame retardant (grade) 4”. It is made of woven fiberglass cloth with an epoxy resin binder that is flame resistant. FR-4 glass epoxy is a popular and versatile high pressure thermoset plastic laminate grade with good strength to weight ratios. With near zero water absorption FR-4 is most commonly used as an electrical insulator possessing considerable mechanical strength. The material is known to retain its high mechanical values and electrical insulating qualities in both dry and humid conditions.

N.E.M.A. - National Electrical Manufacturers Association [28], is the regulating authority for FR-4 and other insulating laminate grades. The typical values for its electrical properties are given in the table below.

Table 4: Electrical properties of Fr-4 substrate

Property	**Typical Value**
Dielectric Breakdown Voltage (0.062”) (D-48/50)	> 54,000 Volts
Electric Strength (0.062”) (D-48/50)	750 V/mil
Dielectric constant \permittivity	4.70 max, 4.35 at 500 MHz, 4.34 at 1 GHz
Dissipation Factor (D24/23)	0.018
Arc Resistance	100 seconds
Moisture Absorption	<0.25%